AMAS Course on Reliability-Based Design and Optimisation
RBO'03 – (pp.99–156) – Warsaw, September 15-18, 2003

Stochastic computational mechanics

C. BUCHER and M. MACKE

Bauhaus–University Weimar
Institute of Structural Mechanics
Marienstrasse. 15, D-99421 Weimar, Germany
christian.bucher@bauing.uni-weimar.de

Recent methods in computational structural mechanics put more emphasis on the consideration of uncertainties of loads and structural properties within the analysis. In most cases, these methods rely heavily on probability theory and statistics. Computational procedures for an efficient handling of random phenomena in structural mechanics have been developed over the last few decades. This includes specific concepts for stochastic finite elements which are based on the possibly very close relation between structural and statistical/stochastic data. The paper starts with a description of essential elements from probability theory. This includes random variables, random vectors, and random fields. Special emphasis is then put on outlining methods to determine structural failure probabilities under static and dynamic loading conditions. These methods cover accurate methods such as Monte Carlo simulation as well as approximate methods such as the first order reliability method or the response surface method. Several numerical examples from different areas of structural mechanics demonstrate the application of these methods.

Key words: *Reliability analysis, nonlinear structural analysis, stochastic mechanics, random fields, computational mechanics, stochastic finite elements.*

1. Introduction

Numerical methods for structural analysis have been developed quite substantially over the last decades. In particular, finite element methods and closely related approximations have become state of the art. The modeling capabilities and the solution possibilities lead, on the one hand, to an increasing refinement allowing for more and more details to be captured in the analysis. On the other hand, however, the need for more precise input data becomes urgent in order to avoid or reduce possible modeling errors. Such errors could eventually render the entire analysis procedure useless. Typically, not all uncertainties encountered in structural analysis can be reduced by

http://rcin.org.pl

careful modeling since their source lies in the intrinsic randomness of natural phenomena. It is therefore appropriate to utilize methods based on probability theory to assess such uncertainties and to quantify their effect on the outcome of structural analysis.

The paper presents an overview of probability-based methods to describe structural uncertainties and to calculate stochastic structural responses – in particular structural reliability. The theoretical concepts are supplemented by several numerical examples in which the implementation of the methods in structural mechanics is demonstrated.

2. Random variables

2.1. Basic definitions

Probability in the mathematical sense is defined as a positive measure in the range $[0, 1]$ associated with an event A in probability space. For most physical phenomena this event is defined by the occurrence of a real-valued random value X which is smaller than a prescribed, deterministic value x, i.e.,

$$A = \{X : X < x\}. \tag{2.1}$$

The probability $P(A)$ associated with this event obviously depends on the magnitude of the prescribed value x, i.e., $P(A) = F(x)$. For real valued X and x, this function is called *cumulative distribution function* with

$$F(x) = P(X < x). \tag{2.2}$$

Since for real-valued variables x it is always true that $-\infty < x < \infty$, we obviously have

$$\lim_{x \to -\infty} F(x) = 0, \quad \text{and} \quad \lim_{x \to +\infty} F(x) = 1. \tag{2.3}$$

Formal differentiation of $F(x)$ with respect to x yields the *probability density function*

$$f(x) = \frac{\mathrm{d}}{\mathrm{d}x} F(x). \tag{2.4}$$

From the above relations it follows that the area under the probability density curve must be equal to unity, i.e.,

$$\int_{-\infty}^{\infty} f(x)\mathrm{d}x = 1. \tag{2.5}$$

A qualitative representation of these relations is given in Fig. 1.

http://rcin.org.pl

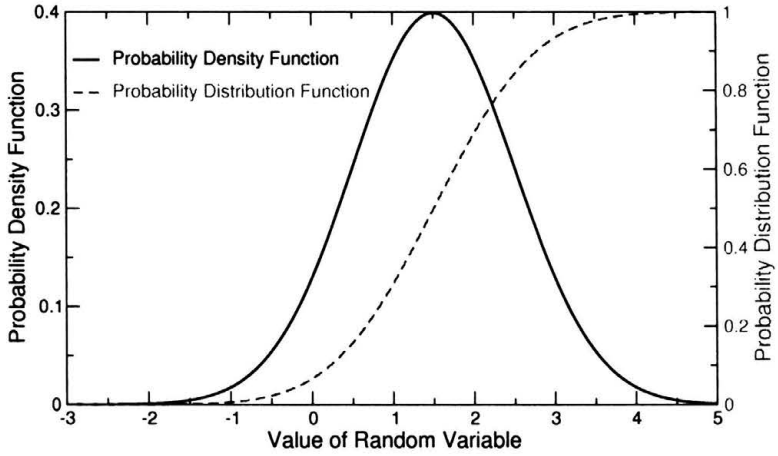

FIGURE 1. Schematic sketch of cumulative distribution and probability density functions.

In many cases it is more convenient to characterize random variables in terms of expected values rather than distribution functions. Special cases of expected values are the *mean value* μ

$$\mu = \mathrm{E}[X] = \int_{-\infty}^{\infty} x f(x) \mathrm{d}x, \tag{2.6}$$

and the *variance* σ^2 of a random variable

$$\sigma^2 = \mathrm{Var}[X] = \mathrm{E}[(X-\mu)^2] = \int_{-\infty}^{\infty} (x-\mu)^2 f(x) \mathrm{d}x. \tag{2.7}$$

The positive square root of the variance σ is called *standard deviation*. For variables with non-zero mean value ($\mu \neq 0$) it is useful to define the dimensionless *coefficient of variation*

$$v = \frac{\sigma}{\mu}. \tag{2.8}$$

A description of random variables in terms of mean value and standard deviation is sometimes called *second moment representation*. Note that the mathematical expectations as defined here are *ensemble averages*, i.e., averages over all possible realizations. For a more extensive treatment of the above subjects see, e.g., [1].

http://rcin.org.pl

2.2. Two types of distributions

Due to its simplicity, the *normal* or *Gaussian* distribution is frequently used. A random variable X is called to be normally distributed when its probability density function $f(x)$ is of the form

$$f(x) = \frac{1}{\sigma}\varphi\left(\frac{x-\mu}{\sigma}\right) = \frac{1}{\sigma\sqrt{2\pi}}\exp\left[-\frac{(x-\mu)^2}{2\sigma^2}\right], \quad -\infty < x < \infty, \tag{2.9}$$

whereby $\varphi(\cdot)$ denotes the *standard* normal density function

$$\varphi(u) = \frac{1}{\sqrt{2\pi}}\exp\left[-\frac{u^2}{2}\right], \quad -\infty < u < \infty. \tag{2.10}$$

The cumulative distribution function $F(x)$ is described by the normal integral $\Phi(\cdot)$ as

$$F(x) = \Phi\left(\frac{x-\mu}{\sigma}\right) \tag{2.11}$$

in which

$$\Phi(u) = \frac{1}{\sqrt{2\pi}}\int_{-\infty}^{u}\exp\left[-\frac{z^2}{2}\right]\mathrm{d}z. \tag{2.12}$$

This integral is not solvable in closed form, however tables and convenient numerical approximations exist. The use of the normal distribution is frequently motivated by the *central limit theorem* which states that an additive superposition of independent random effects tends asymptotically to the normal distribution.

A random variable X is referred to as *lognormally* distributed when its probability density function $f(x)$ is

$$\begin{aligned} f(x) &= \frac{1}{a(x-x_0)}\varphi\left(\frac{\ln[x-x_0]-b}{a}\right) \\ &= \frac{1}{a(x-x_0)\sqrt{2\pi}}\exp\left[-\frac{(\ln[x-x_0]-b)^2}{2a^2}\right], \quad x_0 \le x < \infty, \end{aligned} \tag{2.13}$$

and its cumulative distribution function $F(x)$ is consequently given by

$$F(x) = \Phi\left(\frac{\ln[x-x_0]-b}{a}\right). \tag{2.14}$$

In other words, a random variable X is said to be lognormal when its logarithm is normally distributed. In the above equations, the parameters a and b are related to the mean value μ and the standard deviation σ of X by

$$a = \sqrt{\ln\left[\frac{\sigma^2}{(\mu-x_0)^2}+1\right]} \quad \text{and} \quad b = \ln[\mu-x_0] - \frac{a^2}{2} \tag{2.15}$$

http://rcin.org.pl

or

$$\mu = x_0 + \exp\left[b + \frac{a^2}{2}\right] \quad \text{and} \quad \sigma = \exp\left[b + \frac{a^2}{2}\right] \sqrt{\exp[a^2] - 1}. \tag{2.16}$$

In Fig. 2 the normal and lognormal probability density functions are displayed for $\mu = 1.0$ and $\sigma = 0.5$. It is clearly seen that the lognormal density function is non-symmetric.

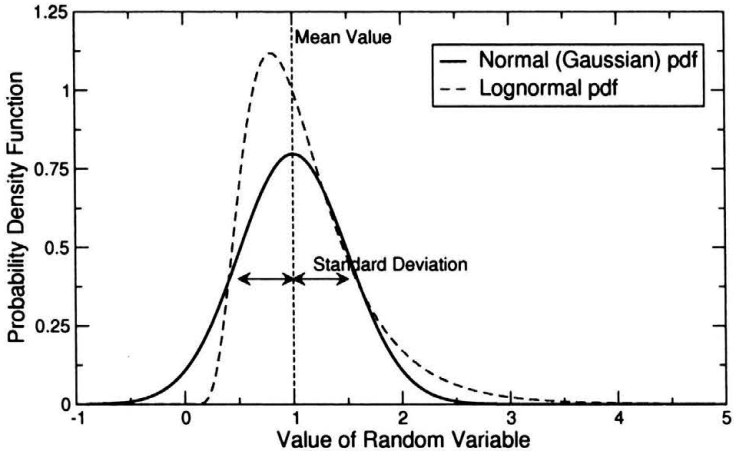

FIGURE 2. Normal and lognormal probability density functions.

2.3. Random vectors

In many applications a large number of random variables occur together. It is conceptually helpful to assemble these random variables X_i (with $i = 1, 2, \ldots, n$) into a *random vector*

$$\mathbf{X} = [X_1, X_2, \ldots, X_n]' \tag{2.17}$$

where $[\cdot]'$ is transpose. For this vector, expected values can be defined in terms of expected values for all of its components, i.e., the mean value vector is defined as

$$\boldsymbol{\mu} = \mathrm{E}[\mathbf{X}] = \big[\mathrm{E}[X_1], \mathrm{E}[X_2], \ldots, \mathrm{E}[X_n]\big]' = [\mu_1, \mu_2, \ldots, \mu_n]', \tag{2.18}$$

and the covariance matrix as

$$\mathbf{C} = \mathrm{Cov}[\mathbf{X}, \mathbf{X}] = \mathrm{E}\big[(\mathbf{X} - \boldsymbol{\mu})(\mathbf{X} - \boldsymbol{\mu})'\big]. \tag{2.19}$$

http://rcin.org.pl

The dimensionless quantity (with $i, j = 1, 2, \ldots, n$)

$$\rho_{ij} = \frac{\mathrm{Cov}[X_i, X_j]}{\sqrt{\mathrm{Var}[X_i]\mathrm{Var}[X_j]}} = \frac{\mathrm{E}\big[(X_i - \mu_i)(X_j - \mu_j)\big]}{\sigma_i \sigma_j} \tag{2.20}$$

is called *coefficient of correlation*, whereby σ_i and σ_j denote the standard deviations of the random variables X_i and X_j, respectively. The value of the coefficient of correlation is bounded in the interval $[-1, 1]$.

The covariance matrix $\mathbf{C}$ is symmetric and positive definite. Therefore, it can be factored into (Cholesky decomposition)

$$\mathbf{C} = \mathbf{L}\mathbf{L}' \tag{2.21}$$

in which $\mathbf{L}$ is a non-singular lower triangular matrix. The Cholesky factor $\mathbf{L}$ can be utilized for a representation of the random variables $\mathbf{X}$ in terms of zero-mean uncorrelated random variables $\tilde{\mathbf{X}}$ via

$$\tilde{\mathbf{X}} = \mathbf{L}^{-1}\big(\mathbf{X} - \mathrm{E}[\mathbf{X}]\big) \quad \text{or} \quad \mathbf{X} = \mathbf{L}\tilde{\mathbf{X}} + \mathrm{E}[\mathbf{X}]. \tag{2.22}$$

2.4. Joint probability density function models

If all n random variables X_i (with $i = 1, 2, \ldots, n$) are mutually independent, then the n-dimensional joint probability density function $f_n(\mathbf{x})$ is given by the product of the individual probability density functions $f(x_i)$, i.e.,

$$f_n(\mathbf{x}) = \prod_{i=1}^{n} f(x_i). \tag{2.23}$$

This follows from the multiplication rule for independent events. Especially for n independent standard normal random variables U_i (with $i = 1, 2, \ldots, n$) follows that

$$\varphi_n(\mathbf{u}) = \prod_{i=1}^{n} \varphi(u_i). \tag{2.24}$$

It should be noted, that independent random variables are always uncorrelated. The reverse is not necessarily true. However, if the random variables are jointly normally distributed, and they are pairwise uncorrelated, then they are also pairwise independent.

If the n jointly normally distributed random variables $\mathbf{X}$ are pairwise correlated, then their joint probability density function is given as

$$f_n(\mathbf{x}, \boldsymbol{\mu}, \mathbf{C}) = \frac{1}{\sqrt{(2\pi)^n \det \mathbf{C}}} \exp\left[-\frac{1}{2}(\mathbf{x} - \boldsymbol{\mu})'\mathbf{C}^{-1}(\mathbf{x} - \boldsymbol{\mu})\right] \tag{2.25}$$

http://rcin.org.pl

or for standardized normal random variates

$$\varphi_n(\mathbf{u}, \mathbf{R}) = \frac{1}{\sqrt{(2\pi)^n \det \mathbf{R}}} \exp\left[-\frac{1}{2}\mathbf{u}' \mathbf{R}^{-1}\mathbf{u}\right], \tag{2.26}$$

with $\mathbf{R}$ denoting the correlation matrix, i.e., the matrix of correlation coefficients.

For random variables $\mathbf{X}$ with arbitrary (marginal) distribution functions $f(x_i)$, an analogous description of the joint probability density function $f_n(\mathbf{x})$ in terms of its marginals and second moment characteristics – i.e., mean $\boldsymbol{\mu}$ and covariance $\mathbf{C}$ – can be achieved in form of the Johnson translation system [2, 3] which is defined as

$$f_n(\mathbf{x}) = \frac{f(x_1, \mu_1, \sigma_1) f(x_2, \mu_2, \sigma_2) \cdots f(x_n, \mu_n, \sigma_n)}{\varphi(u_1)\varphi(u_2)\cdots\varphi(u_n)} \varphi_n(\mathbf{u}, \mathbf{R}). \tag{2.27}$$

In Eq. (2.27) the variables U_i (with $i = 1, 2, \ldots, n$) are zero-mean standard normal random variables given by the translation

$$u_i = \Phi^{-1}[F(x_i, \mu_i, \sigma_i)]. \tag{2.28}$$

As can be seen from Eq. (2.27), the correlation of the random variables $\mathbf{X}$ is handled by the n-dimensional joint normal distribution $\varphi_n(\cdot)$. Since the marginal transformation of Eq. (2.28) changes the correlation structure, the relation between the correlation coefficients ϱ_{ij} in the original random variable space and the correlation coefficients r_{ij} in the normal random variable space is given by

$$\varrho_{ij} = \int_{-\infty}^{\infty} \frac{(x_i - \mu_i)}{\sigma_i} \frac{(x_j - \mu_j)}{\sigma_j} f(x_i) f(x_j) \frac{\varphi_2(u_i, u_j, r_{ij})}{\varphi(u_i)\varphi(u_j)} \mathrm{d}x_i \mathrm{d}x_j. \tag{2.29}$$

Therefore, when using this model, we have to adapt the correlation coefficients r_{ij} by solving Eq. (2.29). This is usually achieved by iteration. A known problem of the model is that this iteration may lead to a non-positive-definite matrix of correlation coefficients in normal random variable space, although the corresponding covariance matrix in original random variable space is positive definite. In this case, the model is not applicable.

The above model is especially convenient when transforming correlated non-normal variables $\mathbf{X}$ to uncorrelated normal variables $\tilde{\mathbf{U}}$ with zero mean and unit variance. This is a common feature in most reliability analysis methods like the first order reliability method, as will be seen below. In this case the transformation consists of the following two steps:

http://rcin.org.pl

1. Transform from correlated non-normal space (variables X_i) to correlated standard normal space (variables U_i) by utilizing the marginal transformation

$$u_i = \Phi^{-1}[F(x_i)], \quad i = 1, 2, \ldots, n. \tag{2.30}$$

   It should be noted that these transformations can be carried out independently.

2. Transform from correlated normal space to standard normal space by means of

$$\tilde{\mathbf{U}} = \mathbf{L}^{-1}\mathbf{U}. \tag{2.31}$$

   in which $\mathbf{L}$ is calculated from the Cholesky decomposition of the correlation matrix $\mathbf{R}$ in normal random variable space.

The transformation from uncorrelated normal to correlated non-normal space is simply made in reverse order.

3. Structural reliability analysis

3.1. Limit state function and probability of failure

Generally, failure (i.e., an undesired or unsafe state of the structure) is defined in terms of a *limit state* function $g(\cdot)$. Having given a vector of n random variables $\mathbf{X} = [X_1, X_2, \ldots, X_n]'$, the limit state function $g(\mathbf{x})$ divides the random variable space in a safe domain

$$S = \{\mathbf{x} : g(\mathbf{x}) > 0\}, \tag{3.1}$$

and a failure domain

$$F = \{\mathbf{x} : g(\mathbf{x}) \leq 0\}. \tag{3.2}$$

Frequently, $Z = g(\mathbf{X})$ is called *safety margin*. As can be seen in Fig. 3, the definition of the limit state function is not unique. However, the probability of failure, i.e., the probability that failure will occur, which is defined as

$$P(F) = P\big(g(\mathbf{X}) \leq 0\big) = \int_{g(\mathbf{x})\leq 0} \cdots \int f(\mathbf{x})\mathrm{d}\mathbf{x} \tag{3.3}$$

is a *unique* quantity. In other words, the probability of failure does not depend on the particular choice of the limit state function.

http://rcin.org.pl

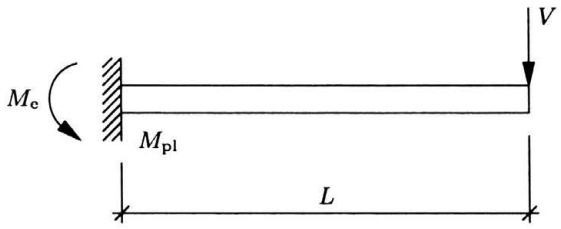

$$F = \{(V, L, M_{pl}) : VL \leq M_{pl}\} = \{(V, L, M_{pl}) : 1 - (VL/M_{pl}) \leq 0\}$$

FIGURE 3. Structural system and failure condition.

3.2. First order second moment (FOSM)

The *first order second moment method* [4, 5] aims at a representation of the limit state function $g(\cdot)$ by calculating the statistical moments of the safety margin Z. Let us assume that the limit state function $g(\cdot)$ is given as

$$Z = g(\mathbf{X}) = g(X_1, X_2, \ldots, X_n) \tag{3.4}$$

where X_i (with $i = 1, 2, \ldots, n$) are random variables. A special case of the limit state function given in Eq. (3.4) is the linear function

$$Z = \alpha_0 + \sum_{i=1}^{n} \alpha_i X_i \tag{3.5}$$

with α_i (with $i = 0, 1, \ldots, n$) being arbitrary constants. Therewith the mean value of Z is given as

$$\mathrm{E}[Z] = \alpha_0 + \sum_{i=1}^{n} \alpha_i \mathrm{E}[X_i] = \alpha_0 + \sum_{i=1}^{n} \alpha_i \mu_i, \tag{3.6}$$

whereas the variance is

$$\mathrm{Var}[Z] = \sum_{i=1}^{n}\sum_{j=1}^{n} \alpha_i \alpha_j \mathrm{Cov}[X_i, X_j] = \sum_{i=1}^{n}\sum_{j=1}^{n} \alpha_i \alpha_j \varrho_{ij} \sigma_i \sigma_j. \tag{3.7}$$

As can be easily seen, the *safety* or *reliability index* β is given by

$$\beta = \frac{\mathrm{E}[Z]}{\sqrt{\mathrm{Var}[Z]}}. \tag{3.8}$$

http://rcin.org.pl

In general, however, $g(\mathbf{x})$ is non-linear. In this case, the mean and variance of Z have to be approximated. Let us assume the function $g(\cdot)$ is suffciently smooth near the expansion point $\mathbf{x}_0$, then

$$g(\mathbf{x}) = g(\mathbf{x}_0) + \sum_{i=1}^{n} \left.\frac{\partial g(\mathbf{x})}{\partial x_i}\right|_{\mathbf{x}=\mathbf{x}_0} (x_i - x_{0,i}) + \cdots . \tag{3.9}$$

Utilizing the mean $\mathbf{x}_0 = \boldsymbol{\mu}$ as an expansion point will result in

$$\mathrm{E}[Z] \approx g(\boldsymbol{\mu}) = g(\mu_1, \mu_2, \ldots, \mu_n) \tag{3.10}$$

and

$$\mathrm{Var}[Z] \approx \sum_{i=1}^{n}\sum_{j=1}^{n} \left.\frac{\partial g(\mathbf{x})}{\partial x_i}\right|_{\mathbf{x}=\boldsymbol{\mu}} \left.\frac{\partial g(\mathbf{x})}{\partial x_j}\right|_{\mathbf{x}=\boldsymbol{\mu}} \mathrm{Cov}[X_i, X_j] . \tag{3.11}$$

Therewith the approximate safety index is

$$\beta \approx \beta^{\mathrm{C}} = g(\boldsymbol{\mu}) \left[\sum_{i=1}^{n}\sum_{j=1}^{n} \left.\frac{\partial g(\mathbf{x})}{\partial x_i}\right|_{\mathbf{x}=\boldsymbol{\mu}} \left.\frac{\partial g(\mathbf{x})}{\partial x_j}\right|_{\mathbf{x}=\boldsymbol{\mu}} \varrho_{ij}\sigma_i\sigma_j\right]^{-1/2} . \tag{3.12}$$

Note that this result does not take into account the types of distributions of the basic variables. The calculated approximate safety index β^{C} also depends significantly on the expansion point for the Taylor-series, as can be seen in the following example.

Given is a cantilever beam of length L with plastic moment m_{pl} under load V (see Fig. 3). Both the load V and the length L are normal random variables. Their statistical description is given in Table 1.

TABLE 1. Definition of random variables for cantilever beam (see Fig. 3).

Variable	Mean	Standard deviation	Distribution
V	5	0.5	Normal
L	2	0.2	Normal
m_{pl}	15	–	–

A possible formulation of the limit state function is

$$g_1(v, l) = m_{\mathrm{pl}} - vl. \tag{3.13}$$

Utilizing the first order second moment method with

$$\frac{\partial g_1(v,l)}{\partial v} = -l \quad \text{and} \quad \frac{\partial g_1(v,l)}{\partial l} = -v, \tag{3.14}$$

http://rcin.org.pl

it follows that

$$g_1(\boldsymbol{\mu}) = 5.0, \tag{3.15}$$

and

$$\left[\frac{\partial g_1(v,l)}{\partial v}\bigg|_{v,l=\boldsymbol{\mu}} \sigma_v\right]^2 + \left[\frac{\partial g_1(v,l)}{\partial l}\bigg|_{v,l=\boldsymbol{\mu}} \sigma_l\right]^2 = 2.0\,. \tag{3.16}$$

Therewith, an approximation for the reliability index is

$$\beta_1^{\mathrm{C}} = \frac{5.0}{\sqrt{2.0}} \approx 3.53\,. \tag{3.17}$$

However, an equivalent formulation for the limit state function is given as

$$g_2(v,l) = \frac{m_{\mathrm{pl}}}{l} - v. \tag{3.18}$$

Therewith

$$\frac{\partial g_2(v,l)}{\partial v} = -1 \quad \text{and} \quad \frac{\partial g_2(v,l)}{\partial l} = -\frac{m_{\mathrm{pl}}}{l^2}, \tag{3.19}$$

and consequently

$$g_2(\boldsymbol{\mu}) = 2.5 \tag{3.20}$$

and

$$\left[\frac{\partial g_2(v,l)}{\partial v}\bigg|_{v,l=\boldsymbol{\mu}} \sigma_v\right]^2 + \left[\frac{\partial g_2(v,l)}{\partial l}\bigg|_{v,l=\boldsymbol{\mu}} \sigma_l\right]^2 \approx 0.81\,. \tag{3.21}$$

The approximate safety index is in this case

$$\beta_2^{\mathrm{C}} = \frac{2.5}{\sqrt{0.81}} \approx 2.78\,, \tag{3.22}$$

which differs clearly from the above calculated approximation β_1^{C}. It should be pointed out that the exact value of the safety index is $\beta = 3.18$.

3.3. First order reliability method (FORM)

The concept of the *first order reliability method* [6, 7] is based on a description of the reliability problem in standard normal space. Hence transformations from dependent non-normal variables to independent normal variables with zero mean and unit variance are required [8]. In the following we assume that we are working in standard normal space. (A possible transformation from non-normal to normal space has been described in Sec. 2.4.)

Let us assume again that the limit state function $g(\cdot)$ is given as

$$g(\mathbf{U}) = g(U_1, U_2, \ldots, U_n) \tag{3.23}$$

http://rcin.org.pl

where U_i (with $i = 1, 2, \ldots, n$) are standard normal random variates. We want now to linearize the limit state function around a point $\mathbf{u}^*$. In first order reliability method the *expansion* or *design point* $\mathbf{u}^*$ is chosen such as to maximize the probability density function of $\mathbf{U}$ in the failure domain (point of maximum likelihood). Geometrically, this coincides for the standard normal space with the point in the failure domain having the minimum distance β from the origin, as shown in Fig. 4. Note that this geometrical formulation is in general not valid in other random variables than the standard normal space.

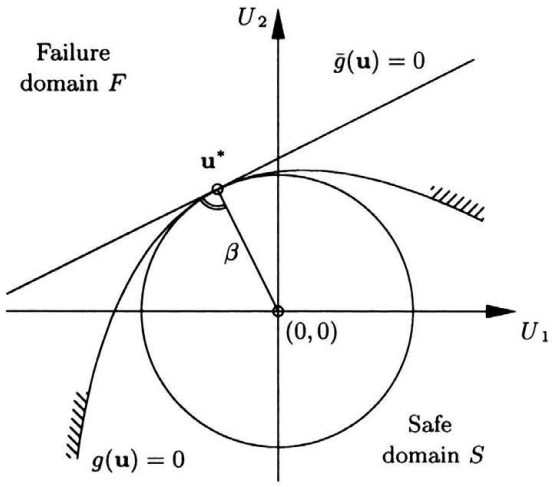

FIGURE 4. Expansion point $\mathbf{u}^*$ and reliability index β in standard normal space.

From the geometrical interpretation of the expansion point $\mathbf{u}^*$ in standard normal space it becomes quite clear that the calculation of the design point and, consequently, the reliability index β can be reduced to an optimization problem of the form

$$\beta = \min \left\{ (\mathbf{u}'\mathbf{u})^{1/2} \mid g(\mathbf{u}) = 0 \right\}, \qquad \beta > 0, \quad g(\mathbf{0}) \in S. \tag{3.24}$$

This leads to the Lagrange function

$$L = \mathbf{u}'\mathbf{u} + \lambda g(\mathbf{u}) \rightarrow \min! \tag{3.25}$$

Standard optimization procedures can be utilized to solve for the location of $\mathbf{u}^*$ [9].

Given is, again, the cantilever beam of length L with plastic moment m_{pl} under load V. Both V and L are normal random variables and their statistical

http://rcin.org.pl

description is the same as given in Table 1. The limit state function is given by

$$g(v,l) = m_{\text{pl}} - vl. \tag{3.26}$$

In standard Gaussian space the Lagrange function is written as

$$L = u_1^2 + u_2^2 + \lambda[m_{\text{pl}} - (u_1\sigma_1 + \mu_1)(u_2\sigma_2 + \mu_2)]\,. \tag{3.27}$$

Therewith, the partial derivatives are

$$\begin{aligned} \partial L/\partial u_1 &= 2u_1 - \lambda\sigma_1(x_2\sigma_2 + \mu_2) = 0, \\ \partial L/\partial u_2 &= 2u_2 - \lambda\sigma_2(x_1\sigma_1 + \mu_1) = 0, \\ \partial L/\lambda &= m_{\text{pl}} - (u_1\sigma_1 + \mu_1)(u_2\sigma_2 + \mu_2) = 0. \end{aligned} \tag{3.28}$$

The solution to the above equation system is given by

$$u_1^* \approx 2.25, \quad u_2^* \approx 2.25, \quad \text{and} \quad \lambda \approx 3.67, \tag{3.29}$$

as can be shown by inserting in Eq. (3.28). This corresponds to a safety index of $\beta = 3.18$. The β-point coordinates in original random variable space are

$$v^* \approx 6.12 \quad \text{and} \quad l^* \approx 2.45\,. \tag{3.30}$$

For determining the failure probability, the exact limit state function $g(\mathbf{u})$ is replaced by a linear approximation $\bar{g}(\mathbf{u})$ as shown in Fig. 4. Expanding the limit state function in $\mathbf{u}^*$ in a Taylor series (with only the linear terms retained) gives

$$\begin{aligned} \bar{g}(\mathbf{u}) &= g(\mathbf{u}^*) + \sum_i (u_i - u_i^*) \left.\frac{\partial g(\mathbf{u})}{\partial u_i}\right|_{\mathbf{u}=\mathbf{u}^*} \\ &= g(\mathbf{u}^*) + (\mathbf{u} - \mathbf{u}^*)'\boldsymbol{\zeta}(\mathbf{u}^*) \end{aligned} \tag{3.31}$$

or simply

$$\bar{g}(\mathbf{u}) = \boldsymbol{\alpha}'\mathbf{u} + \beta = 0. \tag{3.32}$$

In Eq. (3.32) the $\boldsymbol{\alpha}$-values – so called sensitivity factors – are given by

$$\boldsymbol{\alpha}' = \frac{\boldsymbol{\zeta}(\mathbf{u}^*)}{\sqrt{\boldsymbol{\zeta}'(\mathbf{u}^*)\boldsymbol{\zeta}(\mathbf{u}^*)}}, \tag{3.33}$$

whereas the β-index is

$$\beta = \frac{g(\mathbf{u}^*) - (\mathbf{u}^*)'\boldsymbol{\zeta}(\mathbf{u}^*)}{\sqrt{\boldsymbol{\zeta}'(\mathbf{u}^*)\boldsymbol{\zeta}(\mathbf{u}^*)}}. \tag{3.34}$$

http://rcin.org.pl

As can be seen from Eq. (3.32), the linearized limit state function is a linear combination of normally distributed random variables, i.e., the limit state function is also a normal random variable with mean

$$\mathrm{E}[\bar{g}(\mathbf{u})] = \beta \tag{3.35}$$

and variance

$$\mathrm{Var}[\bar{g}(\mathbf{u})] = 1. \tag{3.36}$$

Since failure is defined as $\bar{g}(\mathbf{u}) \leq 0$ the failure probability utilizing the linearized limit state function is

$$P(F) = \Phi(-\beta). \tag{3.37}$$

This result is exact if $g(\mathbf{u})$ is actually linear.

4. Monte Carlo methods

4.1. Plain Monte Carlo simulation

In stochastic structural mechanics we are interested in determining functionals of the form

$$\int_{\mathcal{D}} w(\mathbf{x}) f(\mathbf{x}) \mathrm{d}\mathbf{x} = \mathrm{E}[w(\mathbf{x})], \tag{4.1}$$

whereby $\mathcal{D}$ denotes the integration domain and $f(\mathbf{x})$ is a joint probability density function. The most prominent example of such a functional certainly is the probability of failure

$$P(F) = \int_{g(\mathbf{x})\leq 0} \cdots \int f(\mathbf{x}) \mathrm{d}\mathbf{x}. \tag{4.2}$$

Introducing an indicator function $\mathrm{I}(\cdot)$ that equals one if its argument is true, and zero otherwise, we can write the probability of failure in from of Eq. (4.1) as

$$P(F) = \int_{\mathcal{D}} \mathrm{I}(g(\mathbf{x}) \leq 0) f(\mathbf{x}) \mathrm{d}\mathbf{x} = \mathrm{E}[\mathrm{I}(g(\mathbf{x}) \leq 0)]. \tag{4.3}$$

In order to determine $P(F)$, in principle, all available statistical methods for estimating expected values are applicable. If m independent samples $\mathbf{x}^{(k)}$ (with $k = 1, 2, \ldots, m$) of the n-dimensional random vector $\mathbf{X}$ are available, then the estimator

$$\hat{P}(F) = \hat{\mathrm{E}}[\mathrm{I}(g(\mathbf{x}) \leq 0)] = \sum_{k=1}^{m} \mathrm{I}\big(g(\mathbf{x}^{(k)}) \leq 0\big) \tag{4.4}$$

http://rcin.org.pl

yields a consistent and unbiased estimate of $P(F)$ [10, 11]. The variance of this estimator is given as

$$\mathrm{Var}[\hat{P}(F)] = \frac{1}{m}\,\mathrm{Var}[\mathrm{I}(g(\mathbf{x}) \leq 0)] = \frac{1}{m}\left(P(F) - P^2(F)\right). \tag{4.5}$$

Therefore, for small values of $P(F)$ the variance of its estimator is approximately

$$\mathrm{Var}[\hat{P}(F)] \approx \frac{1}{m}\,P(F). \tag{4.6}$$

The required number m of samples to achieve a certain – most preferably small – value of the variance of the estimate is independent of the dimension n of the problem. However, for small values of $P(F)$ and small values of m the confidence of the estimate is very low as can be seen from Eq. (4.6).

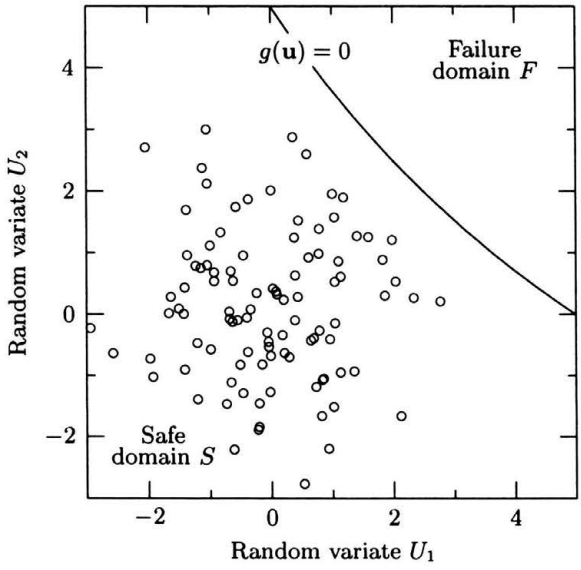

FIGURE 5. Plain Monte Carlo simulation in standard normal space ($m = 100$).

To make this finding more clear, let us re-calculate the cantilever problem of Sec. 3.3 by plain (or crude) Monte Carlo simulation. The dimensionless limit state function in standard normal space is given as (see also Fig. 5)

$$g(u_1, u_2) = m_{\mathrm{pl}} - (u_1\sigma_1 + \mu_1)(u_2\sigma_2 + \mu_2) \tag{4.7}$$

with $m_{\mathrm{pl}} = 15$, $\mu_1 = 2$, $\mu_2 = 5$, $\sigma_1 = 0.2$ and $\sigma_2 = 0.5$. To utilize the estimator of Eq. (4.4), we generate samples of the standard normal variables U_1 and U_2 and evaluate the indicator or limit state function, respectively.

http://rcin.org.pl

As can be seen from Fig. 5, if the estimated probability of failure is quite small, we quite seldom have a hit in the failure domain F. (For the shown $m = 100$ samples there is no hit in the failure domain at all.) In other words, only a small fraction of the samples will contribute to the estimator of the probability of failure and therefore the estimate will have a large variance. For a sample size of $m = 10^4$ we get an estimate of the probability of failure of $\hat{P}(F) = 4.0 \cdot 10^{-4}$ with a sampling error of $\hat{e} = 50.0\,\%$, which is defined as

$$\hat{e} = \frac{\left(\mathrm{Var}[\hat{P}(F)]\right)^{1/2}}{\hat{P}(F)}. \tag{4.8}$$

For a lower number of samples there were no hits in the failure domain, as can be seen from Table 2.

TABLE 2. Comparision of different simulation techniques.

m	**Plain simulation**		**Importance sampling**		**Adaptive sampling**	
	$\hat{P}(F)$	$\hat{e}$	$\hat{P}(F)$	$\hat{e}$	$\hat{P}(F)$	$\hat{e}$
10^2	–	–	$5.9 \cdot 10^{-4}$	19.6 %	$6.8 \cdot 10^{-4}$	8.3 %
10^3	–	–	$6.6 \cdot 10^{-4}$	5.9 %	$6.7 \cdot 10^{-4}$	2.5 %
10^4	$4.0 \cdot 10^{-4}$	50.0 %	$6.9 \cdot 10^{-4}$	1.9 %	$6.7 \cdot 10^{-4}$	0.8 %

4.2. Importance sampling

In order to reduce the standard deviation $(\mathrm{Var}[\hat{P}(F)])^{1/2}$ of the estimator to the order of magnitude of the probability of failure $P(F)$ itself, m must be in the range of $m = (P(F))^{-1}$. For values of $P(F)$ in the range of $1 \cdot 10^{-6}$ this can not be achieved with reasonable computational effort. Alternatively, strategies have top be employed which increase the "hit-rate" by artificially producing more samples in the failure domain than should occur according to the distribution function $f(\mathbf{x})$. One way to approach this solution is the introduction of a positive weighting function $h(\cdot)$ such that

$$P(F) = \int_{\mathcal{D}} \mathrm{I}(g(\mathbf{x}) \leq 0) f(\mathbf{x}) \mathrm{d}\mathbf{x} = \int_{\mathcal{D}} \mathrm{I}(g(\mathbf{x}) \leq 0) \frac{f(\mathbf{x})}{h(\mathbf{x})} h(\mathbf{x}) \mathrm{d}\mathbf{x}. \tag{4.9}$$

This positive weighting function can be interpreted as the density function $h(\tilde{\mathbf{x}})$ of a random vector $\tilde{\mathbf{X}}$. Therewith the probability of failure $P(F)$ is

$$P(F) = \mathrm{E}\left[\mathrm{I}(g(\tilde{\mathbf{x}}) \leq 0) \frac{f(\tilde{\mathbf{x}})}{h(\tilde{\mathbf{x}})}\right]. \tag{4.10}$$

http://rcin.org.pl

The probability of failure is then estimated from [10, 11]

$$\hat{P}(F) = \frac{1}{m}\sum_{k=1}^{m} \mathrm{I}\big(g(\tilde{\mathbf{x}}^{(k)}) \le 0\big)\, \frac{f(\tilde{\mathbf{x}}^{(k)})}{h(\tilde{\mathbf{x}}^{(k)})}. \tag{4.11}$$

This estimator of the failure probability is again unbiased, i.e.,

$$\mathrm{E}[\mathrm{I}(g(\mathbf{x}) \le 0)] = \mathrm{E}\left[\mathrm{I}(g(\tilde{\mathbf{x}}) \le 0)\, \frac{f(\tilde{\mathbf{x}})}{h(\tilde{\mathbf{x}})}\right] \tag{4.12}$$

with variance

$$\mathrm{Var}[\hat{P}(F)] = \frac{1}{m}\left\{\mathrm{E}\left[\mathrm{I}(g(\tilde{\mathbf{x}}) \le 0)\left(\frac{f(\tilde{\mathbf{x}})}{h(\tilde{\mathbf{x}})}\right)^2\right] - (P(F))^2\right\}. \tag{4.13}$$

As can be seen from eqs. (4.12) and (4.13), the utilization of the density function $h(\cdot)$ does not change the value of the estimate of $P(F)$, but only the variance of the estimate. Therefore, a useful choice of $h(\tilde{\mathbf{x}})$ can be based on minimizing the variance of Eq. (4.13). Ideally, such a weighting function should reduce the sampling error. However, this can not be achieved in reality, since such a function should have the property

$$h(\tilde{\mathbf{x}}) = \begin{cases} \dfrac{1}{P(F)}\, f(\tilde{\mathbf{x}}), & \text{if } g(\mathbf{x}) \le 0, \\ 0, & \text{otherwise.} \end{cases} \tag{4.14}$$

This property requires the knowledge of $P(F)$ which, of course, is unknown. Nevertheless, Eq. (4.13) can be utilized to construct improved Monte Carlo estimators as can be seen in the following example.

Let U be normally distributed with cumulative distribution function $\Phi(u)$. Assume that the limit state function is given by

$$g(u) = \beta - u. \tag{4.15}$$

We want to find an optimal sampling density function in the form

$$h(\tilde{u}) = \frac{1}{\sqrt{2\pi}} \exp\left[-\frac{(\tilde{u} - a)^2}{2}\right]. \tag{4.16}$$

In this form, a will be chosen to minimize the variance of the estimated probability of failure.

http://rcin.org.pl

The variance of the estimator of $P(F)$ can be calculated directly by evaluating the expectations given above, i.e.,

$$\begin{aligned}\mathrm{Var}[\hat{P}(F)] &= \frac{1}{m}\int_{\beta}^{\infty}\frac{(f(\tilde{u}))^2}{h(\tilde{u})}\,\mathrm{d}\tilde{u} - \frac{(P(F))^2}{m} \\ &= \frac{1}{m\sqrt{2\pi}}\int_{\beta}^{\infty}\exp\left[-\tilde{u}^2 + \frac{(\tilde{u}-a)^2}{2}\right]\mathrm{d}\tilde{u} - \frac{1}{m}(\Phi(-\beta))^2 \qquad (4.17)\\ &= \frac{1}{m}\exp(a^2)\Phi(-(\beta+a)) - \frac{1}{m}(\Phi(-\beta))^2.\end{aligned}$$

Differentiation with respect to a yields

$$\frac{\partial}{\partial a}\mathrm{Var}[\hat{P}(F)] = \frac{1}{m}\exp(-a^2)\left[2a\Phi(-(\beta+a)) - \varphi(-(\beta+a))\right]. \qquad (4.18)$$

Therefore a necessary condition for the variance $\mathrm{Var}[\hat{P}(F)]$ to become minimal is

$$2a\Phi(-(\beta+a)) - \varphi(-(\beta+a)) = 0. \qquad (4.19)$$

Using the following asymptotic (as $z \to \infty$) approximation for $\Phi(-z)$ (Mill's ratio)

$$\Phi(-z) \approx \frac{1}{z}\varphi(-z) \qquad (4.20)$$

an asymptotic solution to the minimization problem is given by

$$\frac{2a}{\beta+a} - 1 = 0 \quad \text{or} \quad a = \beta. \qquad (4.21)$$

This means that centering the weighting function $h(\tilde{u})$ at the design point $u^* = \beta$ will yield the smallest variance for the estimated failure probability. For a value of $\beta = 3.0$ the variance is reduced by a factor of 164 as compared to plain Monte Carlo simulation.

The above finding can be generalized to n dimensions, leading to *importance sampling at the design point.* This procedure can be established in three steps:

1. Determine the design point $\mathbf{x}^*$ as shown in the context of the first order reliability method in Sec. 3.3.
2. Choose a weighting function (sampling density) $h(\tilde{\mathbf{x}})$ with mean value vector $\mathrm{E}[\tilde{\mathbf{X}}] = \mathbf{x}^*$ and covariance matrix $\mathbf{C} = \mathrm{Cov}[\tilde{\mathbf{X}}, \tilde{\mathbf{X}}] = \mathrm{Cov}[\mathbf{X}, \mathbf{X}]$ in the following form (n-dimensional normal distribution)

$$h(\tilde{\mathbf{x}}) = \frac{1}{\sqrt{(2\pi)^n \det \mathbf{C}}}\exp\left[-\frac{1}{2}(\tilde{\mathbf{x}}-\mathbf{x}^*)'\mathbf{C}^{-1}(\tilde{\mathbf{x}}-\mathbf{x}^*)\right]. \qquad (4.22)$$

http://rcin.org.pl

3. Perform random sampling and statistical estimation according to eqs. (4.11) and (4.13).

The efficiency of this concept depends on the geometrical shape of the limit state function. In particular, limit state functions with high curvatures or almost circular shapes cannot be covered very well.

Applying this procedure again to the cantilever beam problem, we shift the sampling density $h(\cdot)$ to the design point $\mathbf{u}^*$ in standard normal space, i.e., the sampling density is centered around $\mathbf{u}^* = [2.25, 2.25]'$. In Fig. 6 samples generated with this new sampling density are shown. As can be

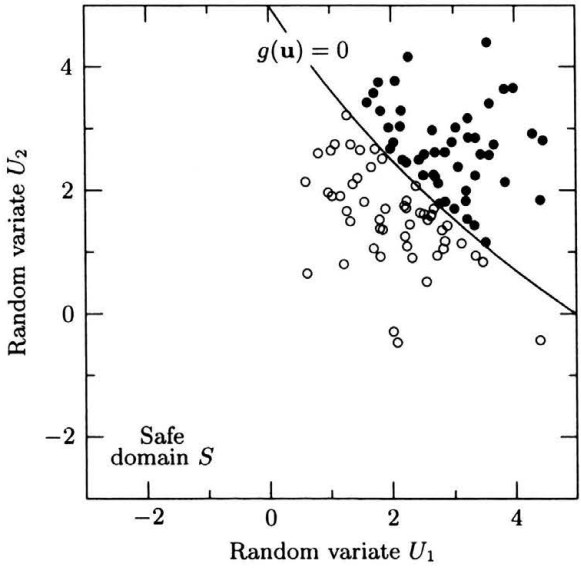

FIGURE 6. Importance sampling at the design point $\mathbf{u}^*$ ($m = 100$).

clearly seen, now approxiamtely half of the samples hit the failure domain, contributing therewith to the estimate of the probability of failure. Since, furthermore, the samples are centered around the most likely point leading to failure, the variance of the estimate can be considerably reduced. For a sample size of $m = 10^3$ the estimate of the probability of failure is $\hat{P}(F) = 5.9 \cdot 10^{-4}$ with a sampling error of $\hat{e} = 5.9\,\%$ (see Table 2).

4.3. Adaptive sampling

Another Monte Carlo method for estimating the probability of failure is *adaptive sampling* [12]. This method also utilizes an importance sampling density function $h(\cdot)$, however, the necessary parameters – like, e.g., the mean

http://rcin.org.pl

values and the covariance matrix – are estimated from the results of a previous Monte Carlo simulation run.

Consider now the sampling density function $h(\tilde{\mathbf{x}}, \boldsymbol{\mu}, \mathbf{C})$ (e.g., a normal joint distribution) with unknown mean values $\boldsymbol{\mu}$ and covariance matrix $\mathbf{C}$. As we already know, an optimal choice of this parameters is given when the variance of estimator of the failure probability becomes minimal. In other words, for determining the mean values $\boldsymbol{\mu}$ and $\mathbf{C}$ the following optimization problem has to be solved

$$\min_{\boldsymbol{\mu},\mathbf{C}} \left[\int_{\mathcal{D}} \mathrm{I}(g(\tilde{\mathbf{x}}) \leq 0) \frac{f^2(\tilde{\mathbf{x}})}{h(\tilde{\mathbf{x}}, \boldsymbol{\mu}, \mathbf{C})} \, \mathrm{d}\tilde{\mathbf{x}} \right]. \tag{4.23}$$

In general it is difficult to find a solution of Eq. (4.23). Therefore, via a first initial guess of the parameters $\hat{\boldsymbol{\mu}}_0$ and $\hat{\mathbf{C}}_0$ samples in the failure domain are generated which allow to estimate these parameters directly and refine them in subsequent steps. In the $(\gamma+1)$-th iteration step the parameters $\hat{\boldsymbol{\mu}}_{\gamma+1}$ and $\hat{\mathbf{C}}_{\gamma+1}$ are estimated by

$$\hat{\boldsymbol{\mu}}_{\gamma+1} = \frac{1}{m} \sum_{k=1}^{m} \tilde{\mathbf{x}}^{(k)} \, \mathrm{I}(g(\tilde{\mathbf{x}}^{(k)}) \leq 0) \frac{f(\tilde{\mathbf{x}}^{(k)})}{h(\tilde{\mathbf{x}}^{(k)}, \hat{\boldsymbol{\mu}}_\gamma, \hat{\mathbf{C}}_\gamma)} \tag{4.24}$$

and

$$\begin{aligned} \hat{\mathbf{C}}_{\gamma+1} = \frac{1}{m} \sum_{i=1}^{m} & (\tilde{\mathbf{x}}^{(k)} - \hat{\boldsymbol{\mu}}_{\gamma+1})(\tilde{\mathbf{x}}^{(k)} - \hat{\boldsymbol{\mu}}_{\gamma+1})' \\ & \times \mathrm{I}(g(\tilde{\mathbf{x}}^{(k)}) \leq 0) \frac{f(\tilde{\mathbf{x}}^{(k)})}{h(\tilde{\mathbf{x}}^{(k)}, \hat{\boldsymbol{\mu}}_\gamma, \hat{\mathbf{C}}_\gamma)} . \end{aligned} \tag{4.25}$$

In other words, adaptive sampling utilizes previously gathered information about the failure domain to improve the estimated parameters and therewith the efficiency of the importance sampling technique.

In Fig. 7 the samples after adaptation are shown. The estimated values of the second moments are $\hat{\mu}_1 = 2.44$, $\hat{\mu}_2 = 2.44$, $\hat{\sigma}_1 = 0.66$, $\hat{\sigma}_2 = 0.66$, $\hat{\varrho}_{12} = -0.88$. Therewith, we can achieve already with a sample size of $m = 10^3$ an estimator of the probability of failure of $\hat{P}(F) = 6.7 \cdot 10^{-4}$ with a high confidence, since the sampling error is only $\hat{e} = 2.5\,\%$, as can be seen from Table 2.

http://rcin.org.pl

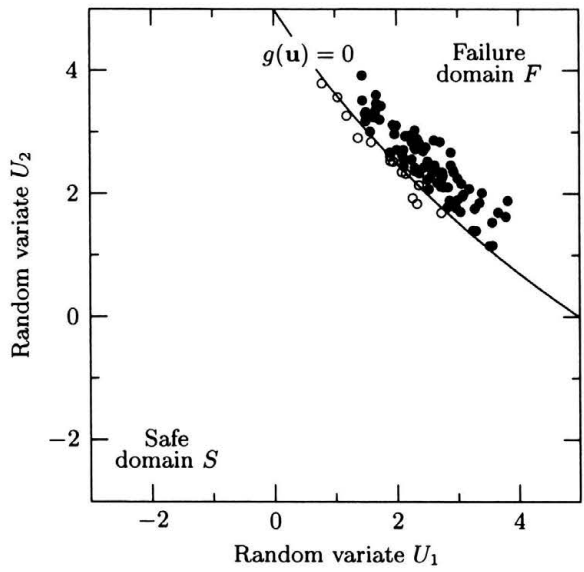

FIGURE 7. Adaptive sampling in standard normal space ($m = 100$).

5. Response surface method

5.1. Response surface models and regression

To reduce computational costs in stochastic structural analysis it has been suggested to utilize the response surface method [13]. Thereto response surfaces are designed as more or less simple mathematical models for describing the possible experimental outcome (e.g., the structural response in terms of displacements, stresses, etc.) of a more or less complex structural system as a function of quantitatively variable factors (e.g., loads or system conditions), which can be controlled by an experimenter. Obviously, the chosen response surface model should give the best possible fit to any collected data.

Let us denote the response of any structural system to a vector $\mathbf{x}$ of n input variables x_i (with $i = 1, 2, \ldots, n$), i.e., $\mathbf{x} = [x_1, x_2, \ldots, x_n]'$, by $z(\mathbf{x})$. In most realistic cases it is quite likely that the *exact* response function will not be known. Therefore, it has to be replaced by a "flexible" function $q(\cdot)$ which will express satisfactorily the relation between the response z and the input variables $\mathbf{x}$. Taking into account a (random) error term ε, then the response can be written over the region of experimentation as

$$z = q(\theta_1, \theta_2, \ldots, \theta_p; x_1, x_2, \ldots, x_n) + \varepsilon, \tag{5.1}$$

whereby θ_j (with $j = 1, 2, \ldots, p$) are the parameters of the approximating

http://rcin.org.pl

function $q(\cdot)$. Taking now expectations, i.e.,

$$\eta = \mathrm{E}[z], \tag{5.2}$$

then the surface represented by

$$\eta = q(\theta_1, \theta_2, \ldots, \theta_p; x_1, x_2, \ldots, x_n) = q(\boldsymbol{\theta}; \mathbf{x}) \tag{5.3}$$

is called a *response surface*. The vector of parameters $\boldsymbol{\theta} = [\theta_1, \theta_2, \ldots, \theta_p]'$ has to be estimated from the experimental data in such a way that Eq. (5.2) is fulfilled. Thereto, the method of maximum likelihood can be utilized. Under the assumption of a normal distribution of the random error terms ε, the method of maximum likelihood can be replaced by the more common method of least squares [14]. In the latter case the parameters $\boldsymbol{\theta}$ are determined in such a way, that the sum of squares of the differences between the value of the response surface $q(\boldsymbol{\theta}; \mathbf{x}^{(k)})$ and the measured response $z^{(k)}$ at the m points of experiment

$$\mathbf{x}^{(k)} = [x_1^{(k)}, \ldots, x_n^{(k)}]', \qquad k = 1, 2, \ldots, m, \tag{5.4}$$

becomes as small as possible. In other words, the sum of squares function

$$s(\boldsymbol{\theta}) = \sum_{k=1}^{m} \left(z^{(k)} - q(\boldsymbol{\theta}; \mathbf{x}^{(k)})\right)^2 \tag{5.5}$$

has to be minimized. This corresponds to a minimization of the variance of the random error terms ε. The minimizing choice of $\boldsymbol{\theta}$ is called a *least-squares estimate* and is denoted by $\hat{\boldsymbol{\theta}}$.

The above regression problem becomes more simple to deal with when the response surface model is linear in its parameters $\boldsymbol{\theta}$. Let us assume that the response surface is given by

$$\eta = \theta_1 q_1(\mathbf{x}) + \theta_2 q_2(\mathbf{x}) + \cdots + \theta_p q_p(\mathbf{x}). \tag{5.6}$$

The observations $z^{(k)}$ made at the points of experiment $\mathbf{x}^{(k)}$ can be represented by this response surface model as

$$\begin{bmatrix} z^{(1)} \\ z^{(2)} \\ \vdots \\ z^{(m)} \end{bmatrix} = \begin{bmatrix} q_1(\mathbf{x}^{(1)}) & q_2(\mathbf{x}^{(1)}) & \cdots & q_p(\mathbf{x}^{(1)}) \\ q_1(\mathbf{x}^{(2)}) & q_2(\mathbf{x}^{(2)}) & \cdots & q_p(\mathbf{x}^{(2)}) \\ \vdots & \vdots & & \vdots \\ q_1(\mathbf{x}^{(m)}) & q_2(\mathbf{x}^{(m)}) & \cdots & q_p(\mathbf{x}^{(m)}) \end{bmatrix} \begin{bmatrix} \theta_1 \\ \theta_2 \\ \vdots \\ \theta_p \end{bmatrix} + \begin{bmatrix} \varepsilon^{(1)} \\ \varepsilon^{(2)} \\ \vdots \\ \varepsilon^{(m)} \end{bmatrix} \tag{5.7}$$

or

$$\mathbf{z} = \mathbf{Q}\boldsymbol{\theta} + \boldsymbol{\varepsilon} \tag{5.8}$$

http://rcin.org.pl

with $\boldsymbol{\varepsilon}$ as a vector of random error terms. Assuming that the random error terms are normally distributed and statistically independent with constant variance σ^2, i.e.,

$$\mathrm{E}\left[\varepsilon^{(k)}\right] = 0, \quad \mathrm{Var}\left[\varepsilon^{(k)}\right] = \sigma^2 \quad \text{and} \quad \mathrm{Cov}\left[\varepsilon^{(k)}, \varepsilon^{(l)}\right] = 0 \quad \text{for} \quad k \neq l, \tag{5.9}$$

then the the covariance matrix of the observations $\mathbf{z}$ is

$$\mathrm{Cov}[\mathbf{z}] = \mathrm{E}\left[(\mathbf{z} - \mathrm{E}[\mathbf{z}])\,(\mathbf{z} - \mathrm{E}[\mathbf{z}])'\right] = \sigma^2 \mathbf{I} \tag{5.10}$$

with $\mathbf{I}$ as an identity matrix.

The least square estimates $\hat{\boldsymbol{\theta}} = [\hat{\theta}_1, \ldots, \hat{\theta}_p]'$ of the parameter vector $\boldsymbol{\theta}$ are determined such that

$$L = (\mathbf{z} - \mathbf{Q}\hat{\boldsymbol{\theta}})'(\mathbf{z} - \mathbf{Q}\hat{\boldsymbol{\theta}}) = \mathbf{z}'\mathbf{z} - 2\,\mathbf{z}'\mathbf{Q}\hat{\boldsymbol{\theta}} + (\mathbf{Q}\hat{\boldsymbol{\theta}})'\mathbf{Q}\hat{\boldsymbol{\theta}} \tag{5.11}$$

becomes minimal. A necessary condition is that

$$\frac{\partial L}{\partial \hat{\boldsymbol{\theta}}} = -2\,\mathbf{z}'\mathbf{Q} + 2\,(\mathbf{Q}\hat{\boldsymbol{\theta}})'\mathbf{Q} = 0. \tag{5.12}$$

From this follows that

$$\mathbf{Q}'\mathbf{Q}\hat{\boldsymbol{\theta}} = \mathbf{Q}'\mathbf{z}. \tag{5.13}$$

The fitted regression model is consequently given by

$$\hat{\mathbf{z}} = \mathbf{Q}\hat{\boldsymbol{\theta}}. \tag{5.14}$$

If the matrix $\mathbf{Q}'\mathbf{Q}$ is not rank deficit, i.e., $\mathrm{rank}\,(\mathbf{Q}'\mathbf{Q}) = p \leq m$, then there exists a unique solution to the above system of equations. The estimated parameter vector is given by

$$\hat{\boldsymbol{\theta}} = \left(\mathbf{Q}'\mathbf{Q}\right)^{-1}\mathbf{Q}'\mathbf{z}. \tag{5.15}$$

This estimator is unbiased, i.e.,

$$\mathrm{E}\left[\hat{\boldsymbol{\theta}}\right] = \boldsymbol{\theta} \tag{5.16}$$

with covariance

$$\mathrm{Cov}[\hat{\boldsymbol{\theta}}] = \sigma^2\left(\mathbf{Q}'\mathbf{Q}\right)^{-1}. \tag{5.17}$$

If the above made assumptions with respect to the random error terms $\boldsymbol{\varepsilon}$ do not hold – e.g. the error terms are correlated or non-normally distributed – then a different minimizing function L than given in Eq. (5.11) has to be utilized. Typical examples thereof are given in [14].

http://rcin.org.pl

5.2. Analysis of variance

Since a response surface is only an approximation of the functional relationship between the structural response and the basic variables, it should be evident that, in general, there is always some *lack of fit* present. Therefore, a crucial point when utilizing response surfaces is to check whether the achieved fit of the response surface model to the experimental data suffices or if the response surface model has to be replaced by a more appropriate one. Therefore, different measures have been proposed in the past for testing different aspects of response surface models. The basic principle of these measures is to analyze the variation of the response data in comparison to the variation which can be reproduced by the chosen response surface model – that's why this kind of response surface testing is also referred to as *analysis of variance.*

Let us start with a measure of overall variability in a set of experimental data, the *total sum of squares* s_t. It is defined as the sum of squared differences $(z^{(k)} - \bar{z})$ between the observed experimental data $z^{(k)}$ (with $k = 1, 2, \ldots, m$) and its average value

$$\bar{z} = \frac{1}{m} \sum_{k=1}^{m} z^{(k)}, \tag{5.18}$$

i.e.,

$$s_t = \mathbf{z}'\mathbf{z} - \frac{1}{m} \left(\mathbf{1}'\mathbf{z}\right)^2 \tag{5.19}$$

where $\mathbf{1}$ is a vector of ones. If we divide s_t by the appropriate number of degrees of freedom, i.e., $(m-1)$, we obtain the sample variance of the z's, which is a standard measure of variability.

The total sum of squares can be partitioned into two parts, the *regression sum of squares* s_r, which is the sum of squares explained by the utilized response surface model, and the *error sum of squares* s_e, which represents the sum of squares unaccounted for by the fitted model. The regression sum of squares is defined as as the sum of squared differences $(\hat{z}^{(k)} - \bar{z})$ between the value $\hat{z}^{(k)}$ predicted by the response surface and the average value $\bar{z}$ of the observed data, i.e.,

$$s_r = (\mathbf{Q}\hat{\boldsymbol{\theta}})'\mathbf{z} - \frac{1}{m} \left(\mathbf{1}'\mathbf{z}\right)^2. \tag{5.20}$$

If the response surface model has p parameters, then the number of degrees of freedom associated with the measure s_r is $(p-1)$.

The sum of squares unaccounted for in the model – called error sum of squares or, sometimes also, residual sum of squares – is defined as the squared

http://rcin.org.pl

difference $(z^{(k)} - \hat{z}^{(k)})$ between the observed experimental data $z^{(k)}$ and the value $\hat{z}^{(k)}$ predicted by the response surface, i.e.,

$$s_e = \mathbf{z}'\mathbf{z} - (\mathbf{Q}\hat{\boldsymbol{\theta}})'\mathbf{z}. \tag{5.21}$$

Obviously, the error sum of square s_e is the difference between the total sum of squares s_t and the regression sum of squares s_r, i.e. $s_e = s_t - s_r$. Consequently, the degrees of freedom associated with the measure s_e are $(m-p) = (m-1) - (p-1)$. Moreover, it can be shown that

$$\mathrm{E}[s_e] = \sigma^2(m-p). \tag{5.22}$$

Thus an unbiased estimator of σ^2 is given by

$$\hat{\sigma}^2 = \frac{s_e}{m-p}. \tag{5.23}$$

From the above defined sums of squares different kinds of statistics can be constructed which measure certain aspects of the utilized response surface. The first of such measures is the *coefficient of (multiple) determination*

$$r^2 = \frac{s_r}{s_t} = 1 - \frac{s_e}{s_t} \tag{5.24}$$

which measures the portion of the total variation of the values $z^{(k)}$ about the mean $\bar{z}$ which can be explained by the fitted response surface model. We can easily see that $0 \leq r^2 \leq 1$. A large value of r^2 is supposed to indicate that the regression model is a good one. Unfortunately, adding an additional variable to an existing response surface model will always increase r^2 – independent of its relevancy to the model [15]. Therefore, an adjusted r^2-statistic has been proposed, defined as

$$r_A^2 = 1 - \frac{\mathrm{E}[s_e]}{\mathrm{E}[s_t]} = 1 - \frac{s_e}{s_t}\frac{(m-1)}{(m-p)}. \tag{5.25}$$

As has been pointed out in [15], in general the measure r_A^2 does not increase when terms are added to the model, but in fact decreases often if these additional terms are unnecessary.

A different measure, which allows to test the significance of the fitted regression equation, is the ratio of the mean regression sum of squares and the mean error sum of squares, i.e.,

$$F_0 = \frac{\mathrm{E}[s_r]}{\mathrm{E}[s_e]} = \frac{s_r}{s_e}\frac{(m-p)}{(p-1)}, \tag{5.26}$$

http://rcin.org.pl

the so-called F-statistic, which follows an F-distribution. The F-statistic allows to test the null hypothesis

$$H_0: \quad \theta_1 = \theta_2 = \cdots = \theta_p = 0 \tag{5.27}$$

against the alternative hypothesis

$$H_1: \quad \theta_j \neq 0 \text{ for at least one value of } \theta_j \text{ (with } j = 1, 2, \ldots, p). \tag{5.28}$$

For a specified level of significance α, the hypothesis H_0 is rejected if

$$F_0 > F_{\alpha, p-1, m-p}. \tag{5.29}$$

Here $(p-1)$ is the degrees of freedom numerator and $(m-p)$ is the degrees of freedom denominator. If H_0 is rejected we can conclude that at least one or more of the terms of the response surface model are able to reproduce a large extent of the variation observed in the experimental data. Or, if the hypothesis H_0 is not rejected, a more adequate model has to be selected, since none of the terms in the model seem to be of indispensable nature. Further and more advanced measures or checking procedures can be found, e.g., in [14, 15, 16, 17].

5.3. First- and second-order polynomials

As already mentioned above, response surfaces are designed such, that a complex functional relation between the structural response and the basic variables is described by an appropriate, but – preferably – as simple as possible mathematical model. The term "simple" means in the context of response surfaces, that the model should be continuous in the basic variables and should have a small number of terms, whose coefficients can be easily estimated. Polynomial models of low-order fulfill such demands. Therefore, in the area of reliability assessment the most common response surface models are first- and second-order polynomials (cf. [13, 18, 19, 20]).

The general form of a first-order model of a response surface η, which is linear in its n basic variables x_i, is

$$\eta = \theta_0 + \sum_{i=1}^{n} \theta_i x_i \tag{5.30}$$

with θ_i (with $i = 0, 1, \ldots, n$) as the unknown parameters to be estimated from the experimental data. The parameter θ_0 is the value of the response surface at the origin or the center of the experimental design, whereas the coefficients θ_i represent the gradients of the response surface in the direction

http://rcin.org.pl

of the respective basic variables x_i. As can be seen from Eq. (5.30), the first-order model is not able to represent even the simplest interaction between the input variables.

If it becomes evident that the experimental data can not be represented by a model whose basic variables have independent influences, then the first-order model can be enriched with (simple) interaction terms, such that

$$\eta = \theta_0 + \sum_{i=1}^{n} \theta_i x_i + \sum_{i=1}^{n-1} \sum_{j=i+1}^{n} \theta_{ij} x_i x_j. \tag{5.31}$$

The total number of parameters to be estimated is given by $1 + n(n+1)/2$. In the response surface model of Eq. (5.31) there is some curvature present, but only from the twisting of the planes of the respective input variables. If a substantial curvature is required as well, then the above model can be further enriched by n quadratic terms to a complete second-order model of the form

$$\eta = \theta_0 + \sum_{i=1}^{n} \theta_i x_i + \sum_{i=1}^{n} \sum_{j=i}^{n} \theta_{ij} x_i x_j. \tag{5.32}$$

The total number of parameters to be estimated is, therewith, given by $1 + n + n(n+1)/2$. In most common cases either the first-order or the complete second-order model are utilized as response surface functions.

5.4. Design of experiments

Having chosen an appropriate response surface model, support points $\mathbf{x}^{(k)}$ (with $k = 1, 2, \ldots, m$) have to be selected to estimate in a sufficient way the unknown parameters of the response surface. Thereto, a set of samples of the basic variables is generated. In general, this is done by applying predefined schemes, so called *designs of experiments*. The schemes shown in the following are saturated designs for first- and second-order polynomials, as well as full factorial and central composite designs. As is quite well known from experiments regarding physical phenomena, it is most helpful to set up the experimental scheme in a space of dimensionless variables. The schemes as described in the following perform experimental designs in a space of dimension n, where n is equal to the number of relevant basic variables.

The selected design of experiments provides us with a grid of points defined by the dimensionless vectors $\boldsymbol{\xi}^{(k)} = [\xi_1^{(k)}, \xi_2^{(k)}, \ldots, \xi_n^{(k)}]'$. This grid has to be centered around a vector $\mathbf{c} = [c_1, c_2, \ldots, c_n]'$. In the absence of further knowledge, this center point can be chosen equal to the vector of mean values $\boldsymbol{\mu} = [\mu_1, \mu_2, \ldots, \mu_n]'$ of the basic random variables X_i (with $i = 1, 2, \ldots, n$).

http://rcin.org.pl

As will be shown below, when further knowledge about the reliability problem becomes available other choices of the center point are, in general, more appropriate. The distances from the center are controlled by the scaling vector $\mathbf{s} = [s_1, s_2, \ldots, s_n]'$. In many cases it is useful to choose the elements s_i of this scaling vector equal to the standard deviations σ_i of the random variables X_i. So, in general, a support point $\mathbf{x}^{(k)}$ (with $k = 1, 2, \ldots, m$) is defined as

$$\mathbf{x}^{(k)} = \begin{bmatrix} x_1^{(k)} \\ x_2^{(k)} \\ \vdots \\ x_n^{(k)} \end{bmatrix} = \begin{bmatrix} c_1 + \xi_1^{(k)} s_1 \\ c_2 + \xi_2^{(k)} s_2 \\ \vdots \\ c_n + \xi_n^{(k)} s_n \end{bmatrix}. \tag{5.33}$$

The number m of generated support points depends on the selected method.

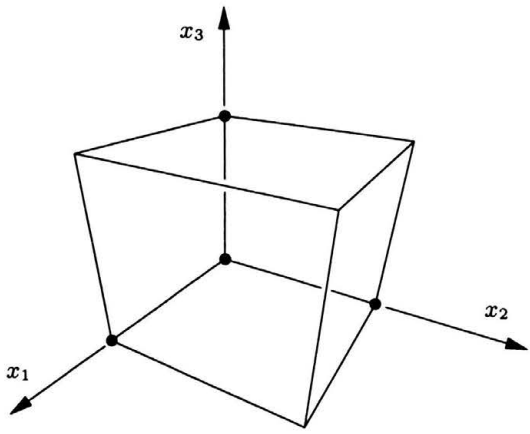

FIGURE 8. Saturated linear experimental scheme for $n = 3$.

Saturated designs provide a number of support points just sufficient to represent a certain class of response functions exactly. Hence for a linear saturated design, a linear function will be uniquely defined. Obviously, $m = n + 1$ samples are required for this purpose (cf. Fig. 8). The factors $\xi_i^{(k)}$ for $n = 3$ are given by

$$\boldsymbol{\xi} = [\boldsymbol{\xi}^{(1)}, \boldsymbol{\xi}^{(2)}, \boldsymbol{\xi}^{(3)}, \boldsymbol{\xi}^{(4)}] = \begin{bmatrix} 0 & +1 & 0 & 0 \\ 0 & 0 & +1 & 0 \\ 0 & 0 & 0 & +1 \end{bmatrix}. \tag{5.34}$$

Here each column represents one support point. Of course, any variation of the factors above in which some or all values of $(+1)$ were replaced by (-1)

http://rcin.org.pl

would also constitute a valid linear saturated design. Obviously, there is some arbitrariness in the design scheme which can usually be resolved only by introducing additional knowledge about the system behavior.

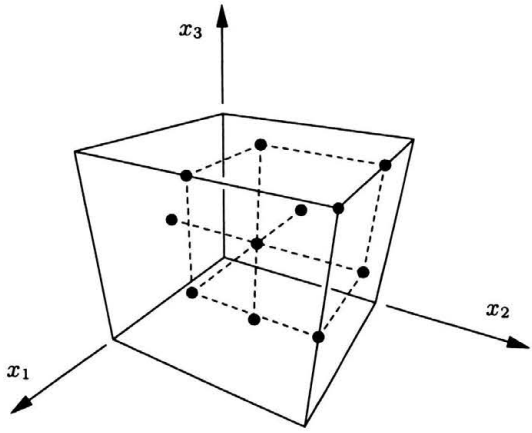

FIGURE 9. Saturated quadratic design scheme for $n = 3$.

A saturated quadratic design (Fig. 9) generates $m = n(n+1)/2 + n + 1$ support points $\mathbf{x}^{(k)}$. The factors $\xi_i^{(k)}$ for $n = 3$ are given by

$$\boldsymbol{\xi} = \begin{bmatrix} 0 & +1 & 0 & 0 & -1 & 0 & 0 & +1 & +1 & 0 \\ 0 & 0 & +1 & 0 & 0 & -1 & 0 & +1 & 0 & +1 \\ 0 & 0 & 0 & +1 & 0 & 0 & -1 & 0 & +1 & +1 \end{bmatrix}. \tag{5.35}$$

Again each column represents one support point. As mentioned above, any change of sign in the pairwise combination would also lead to a saturated design, so that the final choice is somewhat arbitrary and should be based on additional problem-specific information.

Redundant experimental designs provide more support points than required to define the response surface, and thus enable error checking procedures as outlined in the preceding section. Typically, regression is used to determine the coefficients of the basis function. The *full factorial* design (Fig. 10) generates l sample values for each coordinate, thus producing a total of $m = l^n$ support points $\mathbf{x}^{(k)}$ (with $k = 1, 2, \ldots, m$). Note that even for moderate values of l and n this may become prohibitively expensive. Therefore frequently subsets are chosen which leads to *fractional factorial* designs. The *central composite* design (Fig. 11) superimposes a full factorial design with $l = 2$ and a collection of all center points on the faces of an n-dimensional hypercube. Thus it generates $m = (2^n + 2n)$ support points $\mathbf{x}^{(k)}$.

http://rcin.org.pl

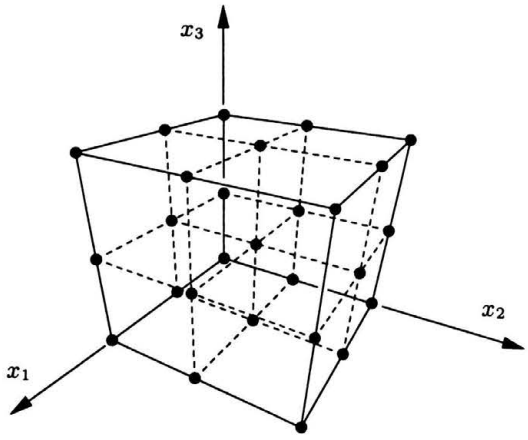

FIGURE 10. Full factorial design scheme for $l = 3$ and $n = 3$.

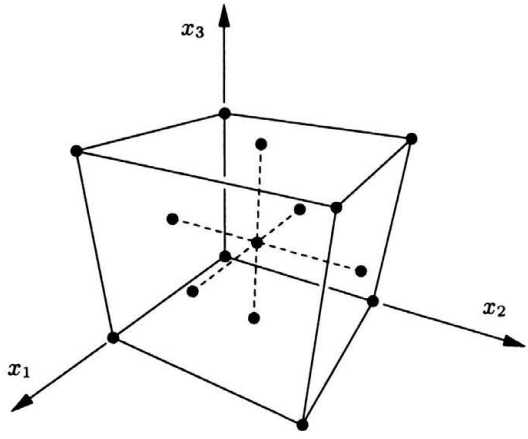

FIGURE 11. Central composite design scheme for $n = 3$.

D-optimal designs attempt to maximize the information content if only a small subset of the otherwise preferable full factorial design can be utilized, e.g., due to restrictions on computer capacity. Given a set of candidate factors $\boldsymbol{\xi}^{(k)}$ a subset of size m' is chosen in order to maximize the following function

$$D = \det(\mathbf{Q}'\mathbf{Q}). \tag{5.36}$$

In this equation, $\mathbf{Q}$ denotes a matrix containing values of the basis functions for the response surface evaluated at the selected support points (cf. Eq. (5.8)). Typically the number m' is chosen to be 1.5-times the corresponding number of a saturated design.

http://rcin.org.pl

TABLE 3. Numbers of support points for different experimental designs.

n	**Linear**	**Quadratic**	**Full factorial** ($l = 2$)	**Central composite**	**Full factorial** ($l = 3$)
1	2	3	2	4	3
2	3	6	4	8	9
3	4	10	8	14	27
4	5	15	16	24	81
5	6	21	32	42	243

Table 3 shows the number of support points as a function of the number of variables for different experimental schemes. It is quite clear that factorial schemes – especially the full factorial – may become quite unattractive due to the exponential growth of the number of support points with increasing dimension of the problem. On the other hand, more economical saturated designs do not allow for sufficient redundancy which is needed to provide error control on the basis of the analysis of variance as outlined in a previous section. Therefore moderately redundant schemes (such as D-optimal designs) may provide the most appropriate solution.

5.5. Adaptation

When applying the response surface method in reliability assessment problems, the response surface has to approximate the limit state function $g(\mathbf{x}) = 0$ sufficiently well in the region which contributes most to the failure probability $P(F)$. In other words, since only a very narrow region around the so-called design point $\mathbf{x}^*$ really contributes to the value of the probability of failure integral, relatively small deviations of the response surface $q(\boldsymbol{\theta}; \mathbf{x})$ from the true limit state function $g(\mathbf{x})$ in this region may lead to significantly erroneous estimates of the probability of failure. In order to avoid this type of error, we must ensure that the "important region" is sufficiently well covered by the design of experiment scheme when constructing the response surface.

Since we do not know the important region beforehand, an adaptation scheme has to be applied which utilizes the information gained from the initial response surface design. In reliability assessment we select the design point $\tilde{\mathbf{x}}^*$ as determined from the first order reliability method utilizing the response surface as a new center point $\mathbf{c}$ for the design scheme. If the region covered by the new design scheme is not overlapping with the initial design scheme region, it is recommendable to perform some additional experiments along the path from the old to the new center point.

A similar adaptation scheme can be constructed by utilizing the basic idea of adaptive sampling. In adaptive sampling the mean value vector $\boldsymbol{\mu}^*$ of

http://rcin.org.pl

the generated samples conditional on the failure domain F is estimated, i.e.,

$$\boldsymbol{\mu}^* = \mathrm{E}[\mathbf{X}|\mathbf{X} \in F]. \tag{5.37}$$

This mean value vector can be utilized – like the design point $\tilde{\mathbf{x}}^*$ above – as a new center point for the design scheme.

Using one of these adaptation schemes will, in general, shift all support points closer to the limit state $g(\mathbf{x}) = 0$. Ideally, some support points should lie on the limit state. A repeated calculation of $\boldsymbol{\mu}^*$ or the design point $\tilde{\mathbf{x}}^*$ can be utilized as an indicator for the convergence of the procedure.

5.6. Example of use of response surface method

Given is a tension bar with known load $p = 1$, random diameter X_1 and yield strength X_2. The dimensionless limit state function is given as

$$g(x_1, x_2) = \frac{\pi x_1^2}{4} x_2 - p = 0. \tag{5.38}$$

The random variables X_1 and X_2 are independent. X_1 is log-normally distributed with distribution function $F(x) = \Phi[(\ln(x) - 1)/2]$, $x > 0$. X_2 obeys the Rayleigh distribution function $F(x) = 1 - \exp[-\pi x^2/(4\mu^2)]$, $x \geq 0$, with mean $\mu = 200$. The response surface model we want to use in the following is a first-order polynomial of the form

$$\eta(\mathbf{u}) = \theta_0 + \theta_1 u_1 + \theta_2 u_2, \tag{5.39}$$

whereas u_1 and u_2, respectively, are the random variables x_1 and x_2 transformed to standard normal space, i.e., $u_i = \Phi^{-1}[F(x_i)]$. As design of experiments we utilize a 2^2-factorial design with one center run in standard normal space, i.e.,

$$\mathbf{u} = \begin{bmatrix} -1 & +1 & -1 & +1 & 0 \\ -1 & -1 & +1 & +1 & 0 \end{bmatrix}. \tag{5.40}$$

As method for adaptation, we determine in each step the design point $\mathbf{u}^* = [u_1^*, u_2^*]'$ for the approximating response surface $\eta(\mathbf{u})$ and repeat the experimental design centered at this design point. As start point we utilize the origin in standard normal space.

When applying this scheme we perform an accompanying analysis of variance, i.e., we determine in each step the coefficient r^2, its adjusted form r_{A}^2 and the F-statistic. As can be seen from Table 4, the above mentioned measures indicate a non-satisfactory performance of the chosen response surface model. Not only differ the values of r^2 and r_{A}^2 considerably from each other,

http://rcin.org.pl

but they are also clearly different from the optimal value of one. This indicates, that the model is not able to reproduce appropriately the variation in the experimental data. Furthermore, when testing the null hypothesis H_0 of Eq. (5.27) at a confidence level of $\alpha = 1\,\%$, we can not reject the hypothesis, since clearly $F_0 < F_{0.01,2,2} = 99$. In other words, the chosen response surface model is not appropriate for the experimentally gained data. This can also be noticed when investigating Fig. 12, which displays the limit state function $g(\mathbf{u})$ in standard normal space for different values of p. As can be seen, the limit state function is highly non-linear.

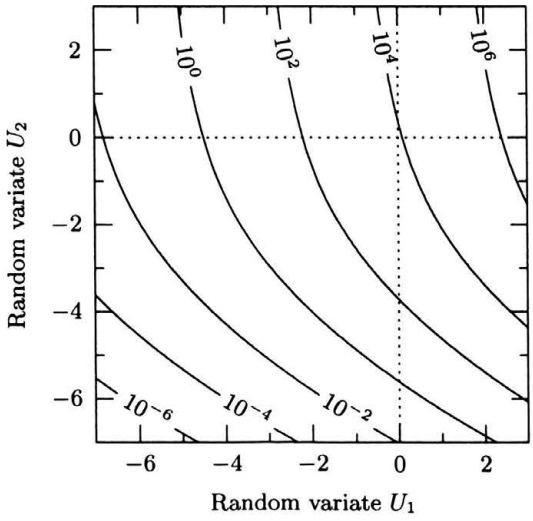

FIGURE 12. Limit state function $g(\mathbf{u})$ in standard normal random variable space for different values of p.

Nevertheless, when taking the logarithm of the response values, a linear response surface would represent a good approximation of the true limit state function. Therefore, a more adequate response surface model would be of the form

$$\eta(\mathbf{u}) = \theta_0 \exp(\theta_1 u_1 + \theta_2 u_2) - 1 \tag{5.41}$$

which can be transformed to its linear form by

$$\tilde{\eta}(\mathbf{u}) = \ln(\eta + 1) = \ln(\theta_0) + \theta_1 u_1 + \theta_2 u_2 = \hat{\theta}_0 + \theta_1 u_1 + \theta_2 u_2. \tag{5.42}$$

When using this response surface model, all measures displayed in Table 4 show satisfactory values. Moreover, already in the second step, i.e., after the first adaptation a reasonable approximation of the exact result can be achieved. The response surface method converges to the point $\mathbf{u}^* =$

http://rcin.org.pl

TABLE 4. Analysis of variance.

	Original scale			Transformed scale		
	1. step	2. step	Last step	1. step	2. step	Last step
s_t	$6.60 \cdot 10^9$	$3.19 \cdot 10^8$	16.95	17.41	19.40	22.90
s_r	$5.04 \cdot 10^9$	$2.38 \cdot 10^8$	10.95	17.40	19.38	22.86
s_e	$1.56 \cdot 10^9$	$0.81 \cdot 10^8$	6.00	0.01	0.02	0.04
r^2	0.76	0.74	0.64	0.99	0.99	0.99
r_A^2	0.53	0.49	0.29	0.99	0.99	0.99
F_0	3.23	2.92	1.82	2044.73	857.02	631.24
u_1^*	−0.68	−1.30	−3.54	−4.10	−3.75	−3.41
u_2^*	−0.37	−0.79	−3.51	−1.21	−1.73	−2.24
β	0.77	1.52	4.98	4.27	4.13	4.08

$[-3.41, -2.24]'$, which relates to a reliability index $\beta = 4.08$. These results are an excellent approximation of the true design-point $\mathbf{u}^* = [-3.46, -2.29]'$ and the true reliability index $\beta = 4.15$. It should also be noted, that when we would have dismissed the indicators in the original scaling as being not relevant, the response surface analysis would not provide a satisfactory result, as can be seen from Table 4.

6. Random fields and stochastic finite elements

6.1. Description of random fields

A *random field* $H(\mathbf{x})$ is a real-valued random variable whose statistics (mean value, standard deviation, etc.) may be different for each value of $\mathbf{x}$ [21, 22], i.e.,

$$H(\mathbf{x}) \in \mathbb{R}, \quad \mathbf{x} = [x_1, x_2, \ldots, x_n]' \in \mathcal{D} \subset \mathbb{R}^n. \tag{6.1}$$

Typical examples of random fields are spatially varying material properties, deviations from a perfect geometry or uncertain structural loads (see Fig. 13). The mean value and auto-covariance function of a random field are given as

$$\mu(\mathbf{x}) = \mathrm{E}[H(\mathbf{x})] \tag{6.2}$$

and

$$c(\mathbf{x}_1, \mathbf{x}_2) = \mathrm{E}\big[\big(H(\mathbf{x}_1) - \mu(\mathbf{x}_1)\big)\big(H(\mathbf{x}_2) - \mu(\mathbf{x}_2)\big)\big] \tag{6.3}$$

respectively. A random field $H(\mathbf{x})$ is called *weakly homogeneous* if

$$\mu(\mathbf{x}) = \text{const.} \ \forall \ \mathbf{x} \in \mathcal{D} \quad \text{and} \quad c(\mathbf{x}, \mathbf{x} + \boldsymbol{\xi}) = c(\boldsymbol{\xi}) \ \ \forall \ \mathbf{x} \in \mathcal{D}. \tag{6.4}$$

http://rcin.org.pl

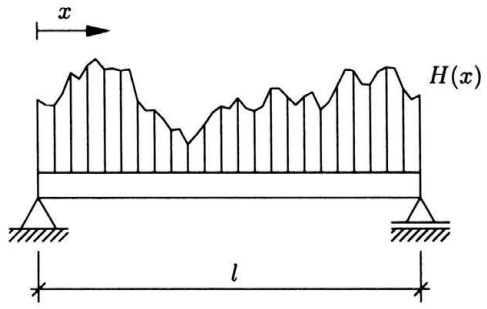

FIGURE 13. Sample function of one-dimensional random field.

A homogeneous random field $H(\mathbf{x})$ is called *isotropic* if

$$c(\mathbf{x}, \mathbf{x} + \boldsymbol{\xi}) = c(\|\boldsymbol{\xi}\|) \quad \forall\, \mathbf{x} \in \mathcal{D}. \tag{6.5}$$

The latter means that the covariance function depends on the distance only (not on the direction). Typically, fiber-reinforced materials are non-isotropic in their mechanical properties. In such a case, the contour lines of constant correlation are elongated in one direction (see Fig. 14).

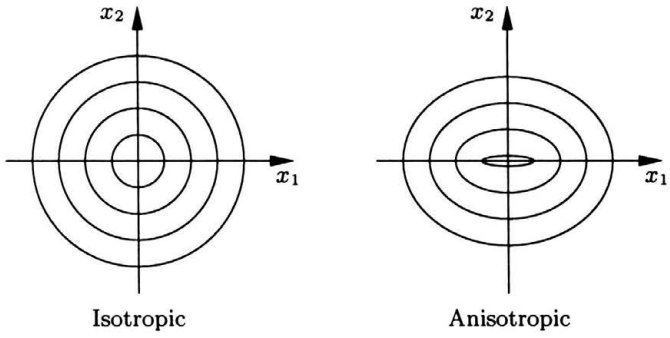

FIGURE 14. Isotropic and anisotropic correlation contours.

For describing random fields, very often the *correlation length* l_c is utilized. Let us define for an isotropic random field $H(\mathbf{x})$ the separation distance δ between two points by

$$\delta = \|\boldsymbol{\xi}\| = \|\mathbf{x}_1 - \mathbf{x}_2\|. \tag{6.6}$$

http://rcin.org.pl

Then the correlation length l_c is given by

$$l_c = \int_0^\infty \delta |c(\delta)| \mathrm{d}\delta \left[\int_0^\infty |c(\delta)| \mathrm{d}\delta \right]^{-1}. \tag{6.7}$$

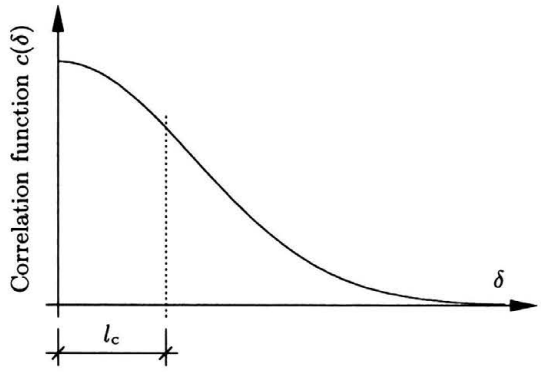

FIGURE 15. Correlation function and correlation length.

6.2. Spectral decomposition

For numerical computations it is useful to represent a continuous random field $H(\mathbf{x})$ in terms of discrete random variables V_k (with $k = 0, 1, \ldots, n$) [23, 24] as

$$H(\mathbf{x}) = \sum_{k=0}^{\infty} V_k \phi_k(\mathbf{x}), \quad \mathbf{x} \in \mathcal{D} \subset \mathbb{R}^n; \; V_k, \phi_k \in \mathbb{R}. \tag{6.8}$$

The functions $\phi_k(\mathbf{x})$ are deterministic spatial shape functions which are usually chosen to represent an orthonormal basis on $\mathcal{D}$. The random coefficients V_k can be made uncorrelated, which is an extension of orthogonality into the random variable case. This representation is usually called *Karhunen-Loéve expansion.* It is based on the following decomposition of the covariance function

$$c(\mathbf{x}_1, \mathbf{x}_2) = \sum_{k=0}^{\infty} \lambda_k \phi_k(\mathbf{x}_1) \phi_k(\mathbf{x}_2) \tag{6.9}$$

in which λ_k and $\phi_k(\cdot)$ are the eigenvalues and eigenfunctions of $c(\cdot, \cdot)$, respectively. These are solutions to the integral equation

$$\int_{\mathcal{D}} c(\mathbf{x}_1, \mathbf{x}_2) \phi_k(\mathbf{x}_1) \mathrm{d}\mathbf{x}_1 = \lambda_k \phi_k(\mathbf{x}_2). \tag{6.10}$$

http://rcin.org.pl

In most finite element applications the random field $H(\mathbf{x})$ is discretized right from the start as

$$H_i = H(\mathbf{x}_i), \quad i = 1, 2, \ldots, n. \tag{6.11}$$

A spectral representation for the discretized random field is then obtained by

$$H_i = \sum_{k=1}^{n} V_k \phi_k(\mathbf{x}_i) = \sum_{k=1}^{n} V_k \phi_{ki}. \tag{6.12}$$

This is equivalent to the following vector-matrix multiplication

$$\mathbf{H} = [\phi_1, \phi_2, \ldots, \phi_n]' \mathbf{V} = \mathbf{\Phi}' \mathbf{V}. \tag{6.13}$$

The columns $\phi_k = [\phi_{k1}, \ldots, \phi_{kn}]'$ of the matrix $\mathbf{\Phi}$ thereby have to fulfill the orthogonality condition

$$\mathbf{\Phi}' \mathbf{\Phi} = \mathbf{I} \tag{6.14}$$

with $\mathbf{I}$ as a unit matrix. The covariance matrix of the coefficients $\mathbf{V} = [V_1, V_2, \ldots, V_k, \ldots, V_n]'$ is given as

$$\mathrm{Cov}[\mathbf{V}, \mathbf{V}] = \mathrm{diag}(\sigma_k^2) \quad \text{with} \quad \sigma_1^2 \geq \sigma_2^2 \geq \ldots \geq \sigma_k^2 \geq \ldots \geq \sigma_n^2. \tag{6.15}$$

The conditions of eqs. (6.14) and (6.15) are satisfied, when the column vectors ϕ_k of the matrix $\mathbf{\Phi}$ are solutions to the following eigenvalue problem

$$\mathrm{Cov}[\mathbf{H}, \mathbf{H}] \phi_k = \sigma_k^2 \phi_k, \quad k = 1, 2, \ldots, n. \tag{6.16}$$

6.3. Stochastic stiffness matrix (plane stress)

The element stiffness matrix $\mathbf{K}^e$ relates the nodal forces $\mathbf{p}^e$ to the nodal displacements $\mathbf{q}^e$ by

$$\mathbf{K}^e \mathbf{q}^e = \mathbf{p}^e \tag{6.17}$$

in which, for the simple element shown in Fig. 16

$$\mathbf{p}^e = \left[p_{x_i}, p_{y_i}, p_{x_j}, p_{y_j}, p_{x_k}, p_{y_k}\right]' \tag{6.18}$$

and

$$\mathbf{q}^e = [u_i, v_i, u_j, v_j, u_k, v_k]'. \tag{6.19}$$

Based on the principle of virtual work, the element stiffness matrix for a linear material law (assuming geometrical linearity as well) is obtained as

$$\mathbf{K}^e = \int_{V^e} \mathbf{B}'(x, y) \mathbf{D}(x, y) \mathbf{B}(x, y) \mathrm{d}V^e. \tag{6.20}$$

http://rcin.org.pl

Typically, the strain interpolation matrix $\mathbf{B}(x,y)$ is chosen in polynomial form, i.e.,

$$\mathbf{B}(x,y) = \sum\sum_{k+l\leq r} \mathbf{B}_{kl} x^k y^l, \quad k,l,r \geq 0. \tag{6.21}$$

In this equation, $\mathbf{B}_{kl}$ are constant matrices. In fact, for the element shown in Fig. 16 there is only one such matrix, i.e., $\mathbf{B}_{00}$.

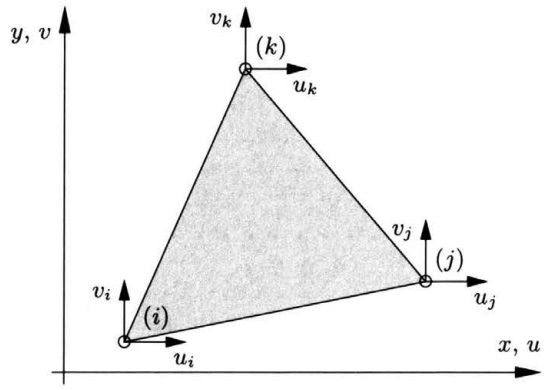

FIGURE 16. Constant strain triangle finite element.

Assuming that the system randomness is described by a random elastic modulus $Y(x,y)$, the elasticity matrix $\mathbf{D}(x,y)$ can be written as

$$\mathbf{D}(x,y) = \mathbf{D}_0 Y(x,y). \tag{6.22}$$

Using the polynomial form of $\mathbf{B}(x,y)$, the element stiffness matrix finally becomes

$$\mathbf{K}^{\mathrm{e}} = \sum\sum_{k+l\leq r}\sum\sum_{m+n\leq r} \mathbf{B}'_{kl}\mathbf{D}_0\mathbf{B}_{mn} \int_{V^{\mathrm{e}}} Y(x,y) x^k y^l x^m y^n \mathrm{d}V^{\mathrm{e}}. \tag{6.23}$$

The last term in this equation is a so-called *weighted integral* of the random field $Y(x,y)$. The global stiffness matrix is then assembled by applying standard finite element techniques.

6.4. Static response (perturbation method)

Let us use a perturbation approach for the random elastic modulus in the form

$$Y(x,y) = Y_0(x,y) + \varepsilon Y_1(x,y) \tag{6.24}$$

http://rcin.org.pl

in which Y_0 is the deterministic mean, ε is a "small" quantity, and Y_1 describes the random deviation from the mean. The assembly of the element stiffness matrices leads to a global stiffness matrix $\mathbf{K}$ which has random perturbations as well, i.e.,

$$\mathbf{K} = \mathbf{K}_0 + \varepsilon \mathbf{K}_1. \tag{6.25}$$

Given the (deterministic) global load vector $\mathbf{p}$, the (random) global displacement vector $\mathbf{q}$ is determined from the solution of the following system of linear equations

$$\mathbf{K}\mathbf{q} = \mathbf{p}. \tag{6.26}$$

Expanding $\mathbf{q}$ into a power series with respect to ε

$$\mathbf{q} = \mathbf{q}_0 + \varepsilon \mathbf{q}_1 + \varepsilon^2 \mathbf{q}_2 + \dots \tag{6.27}$$

an approximate solution can be obtained in terms of powers of ε as

$$\begin{aligned} \varepsilon^0 &: \quad \mathbf{K}_0 \mathbf{q}_0 = \mathbf{p}, \\ \varepsilon^1 &: \quad \mathbf{K}_0 \mathbf{q}_1 = -\mathbf{K}_1 \mathbf{q}_0, \\ \varepsilon^2 &: \quad \dots . \end{aligned} \tag{6.28}$$

Usually, this is truncated at linear terms in ε. From this first order perturbation result the mean value $\mathrm{E}[\mathbf{q}]$ of the displacement vector becomes

$$\mathrm{E}[\mathbf{q}] = \mathbf{q}_0, \tag{6.29}$$

and the covariance matrix of its components is

$$\mathrm{Cov}[\mathbf{q}, \mathbf{q}] = \mathrm{E}[\mathbf{q}_1 \mathbf{q}_1']. \tag{6.30}$$

The actual computation can be based on the weighted integral representation of Eq. (6.23) and takes into account the spectral decomposition of the random fields via Eq. (6.8).

6.5. Natural frequencies of a structure with randomly distributed elastic modulus

In the following, a spherical shell structure (see Fig. 17) in free vibration is considered. The shell is discretized by 288 triangular shell elements [25]. The shell is assumed to be fully clamped along the edge. The material of the shell is assumed to be elastic (in plain stress) and the elastic modulus $Y(\mathbf{x})$ is modeled as a log-normally distributed, homogeneous, and isotropic random field. Its auto-covariance function $c(\mathbf{x}_1, \mathbf{x}_2)$ is assumed to be of the form

$$c(\mathbf{x}_1, \mathbf{x}_2) = \sigma^2 \exp\left[-\frac{\|\mathbf{x}_1 - \mathbf{x}_2\|}{l_c}\right]. \tag{6.31}$$

http://rcin.org.pl

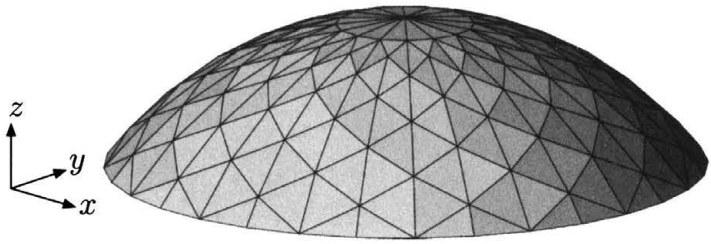

FIGURE 17. Spherical shell structure.

In the above equations, the 3-dimensional vectors $\mathbf{x}_1$ and $\mathbf{x}_2$ are two coordinates of points within the shell structure. The diameter of the shell at the basis is $d = 20\,\mathrm{m}$, the correlation length is assumed to be $l_c = 10\,\mathrm{m}$ and the coefficient of variation of the random field is $v = 0.2$.

The question to be answered is what magnitude of randomness may be expected in the calculated natural frequencies. Quite clearly, this is very important for structural elements designed to carry, e.g., rotating machinery which produces almost harmonic excitation, and possibly resonance. Hence the probability of obtaining high deviations from the mean natural frequency needs to be calculated. This example shows quite typically the close connection required between the stochastic analyses and the finite element analysis. Within the finite element model, the random field $Y(\mathbf{x})$ is represented by its values in the integration points of the elements. The shell elements as utilized here have two layers of each 13 integration points, so there is a total of $26 \times 288 = 7,488$ integration points. In order to reduce this rather high number of random variables the following strategy is applied. First, the elastic modulus is represented by one value per element (given the correlation

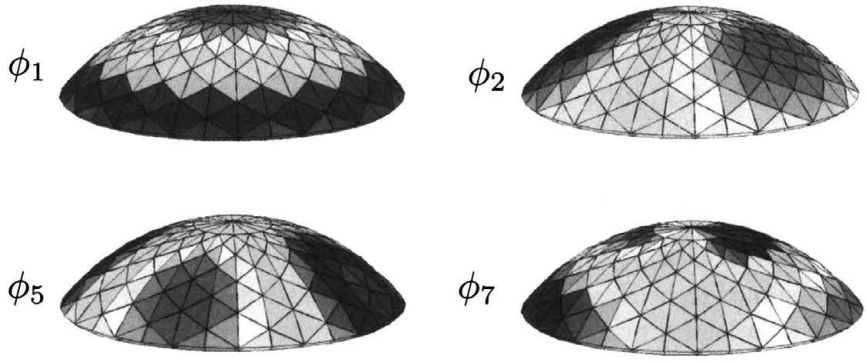

FIGURE 18. Selected mode shapes of the covariance function.

http://rcin.org.pl

length of $l_c = 10\,\mathrm{m}$ this is not a severe simplification). Second, the remaining random field is represented in terms of independent random variables and corresponding space dependent shape functions. These independent variables are obtained by applying the transformation described in Sec. 2.4.

Fig. 18 shows selected space dependent shape functions. They are ordered according to decreasing magnitude of the corresponding eigenvalues. A Monte Carlo simulation is then carried out to generate sample functions of the random field. The simulation results obtained from $m = 10^3$ are shown as a histogram of the fundamental natural frequency in Fig. 19. The results indicate a relatively high scatter of the fundamental frequency – the deterministic system has two equal lowest natural frequencies at 42 Hz – with a coefficient of variation of approximately 15 %.

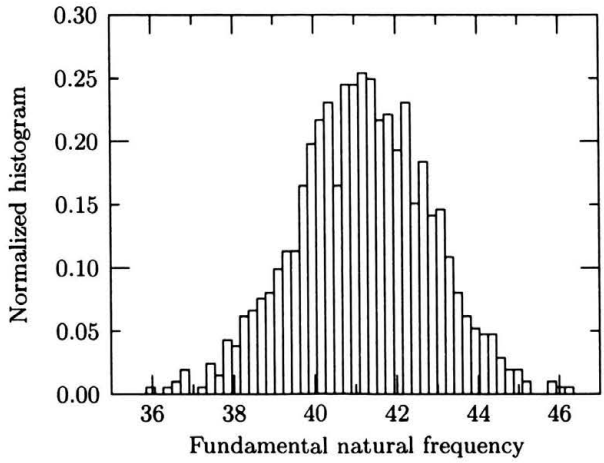

FIGURE 19. Histogram of the fundamental natural frequency.

7. Stability of structures with random imperfections

7.1. Geometrical imperfections

Quite often not only material properties show some considerable scatter, but also the geometry deviates from its nominal value. Such deviations can have a variety of consequences. One of the most pronounced effects can certainly be observed with respect to the degree of stability of slender structures.

Let us assume that the geometrical imperfections are described by a random field $H(\mathbf{x})$ which describes the spatially distributed, random deviations from the perfect geometry at each point $\mathbf{x}$ of the structure. Utilizing the

http://rcin.org.pl

stochastic finite element method, the random field is discretized at n points $H_i = H(\mathbf{x}_i)$ (with $i = 1, \ldots, n$), i.e.,

$$H_i = \sum_{k=1}^{n} V_k \phi_i(\mathbf{x}_i) = \sum_{k=1}^{n} V_k \phi_{ki}. \tag{7.1}$$

If some geometrical points of the structure are not random, but deterministic, the random field has to be conditioned. Let us assume that at the points $\mathbf{S} = [H_1, \ldots, H_p]'$ of the random field the deterministic values $\mathbf{s}$ should be prescribed. Then the conditional random field has to be constructed with the modifed means

$$\mathrm{E}[H_i|\mathbf{s}] = \mathrm{E}[H_i] + \mathrm{Cov}[H_i, \mathbf{S}]\big(\mathrm{Cov}[\mathbf{S}, \mathbf{S}]\big)^{-1}\big(\mathbf{s} - \mathrm{E}[\mathbf{S}]\big), \tag{7.2}$$

and covariances

$$\mathrm{Cov}[H_i, H_j|\mathbf{s}] = \mathrm{Cov}[H_i, H_j] - \mathrm{Cov}[H_i, \mathbf{S}]\big(\mathrm{Cov}[\mathbf{S}, \mathbf{S}]\big)^{-1}\mathrm{Cov}[\mathbf{S}, H_j], \tag{7.3}$$

respectively [26].

7.2. Zero solution and neighbouring paths

The dynamic response of a structure is described by the following equation of motion

$$\mathbf{M}\ddot{\mathbf{q}} + \mathbf{r}(\mathbf{q}, \dot{\mathbf{q}}) = \mathbf{p}(t), \tag{7.4}$$

whereby $\mathbf{M}$ is the mass matrix, $\mathbf{r}(\cdot)$ is a vector of restoring forces and $\mathbf{p}(t)$ is an applied-load vector. Linearization of Eq. (7.4) with respect to the zero solution $(\mathbf{q}_0, \dot{\mathbf{q}}_0)$ results in

$$\begin{aligned} \mathbf{r}(\mathbf{q}, \dot{\mathbf{q}}) \approx \mathbf{r}(\mathbf{q}_0, \dot{\mathbf{q}}_0) &+ \frac{\partial \mathbf{r}}{\partial \dot{\mathbf{q}}}(\mathbf{q}_0, \dot{\mathbf{q}}_0)\,\dot{\bar{\mathbf{q}}} \\ &+ \frac{\partial \mathbf{r}}{\partial \mathbf{q}}(\mathbf{q}_0, \dot{\mathbf{q}}_0)\,\bar{\mathbf{q}} \end{aligned} \tag{7.5}$$

or

$$\mathbf{r}(\mathbf{q}, \dot{\mathbf{q}}) \approx \mathbf{r}(\mathbf{q}_0, \dot{\mathbf{q}}_0) + \mathbf{C}\dot{\bar{\mathbf{q}}} + \mathbf{K}\bar{\mathbf{q}}, \tag{7.6}$$

whereby $\bar{\mathbf{q}} = \mathbf{q} - \mathbf{q}_0$ denotes the perturbation of the zero solution. The quantities $\mathbf{C}$ and $\mathbf{K}$ are the tangential damping and stiffness matrices, respectively. Therewith, the equation of motion (7.4) can be split up in a differential equation for the zero solution

$$\mathbf{M}\ddot{\mathbf{q}}_0 + \mathbf{r}(\mathbf{q}_0, \dot{\mathbf{q}}_0) = \mathbf{p}(t), \tag{7.7}$$

http://rcin.org.pl

and a differential equation for the paths in its neighbourhood, i.e.,

$$\mathbf{M}\ddot{\bar{\mathbf{q}}} + \mathbf{C}\dot{\bar{\mathbf{q}}} + \mathbf{K}\bar{\mathbf{q}} = \mathbf{0}. \tag{7.8}$$

The stability properties of the structure can be determined by analyzing Eq. (7.8).

7.3. Lyapunov exponent

For determining the Lyapunov exponent, Eq. (7.8) is written in state space formulation as

$$\dot{\mathbf{z}} = \begin{bmatrix} \mathbf{0} & \mathbf{I} \\ -\mathbf{M}^{-1}\mathbf{K} & -\mathbf{M}^{-1}\mathbf{C} \end{bmatrix} \mathbf{z} \tag{7.9}$$

or

$$\dot{\mathbf{z}} = \mathbf{A}(t)\mathbf{z}. \tag{7.10}$$

Taking into account the initial conditions $\mathbf{z}(t_0) = \mathbf{z}_0$, the solution for Eq. (7.10) is given by

$$\mathbf{z}(t) = \Lambda(t)\Lambda^{-1}(t_0)\mathbf{z}_0 \tag{7.11}$$

with $\Lambda(\cdot)$ denoting the fundamental matrix of the system (7.10). For periodic coefficients with minimal period T, i.e.,

$$\mathbf{A}(t+T) = \mathbf{A}(t) \tag{7.12}$$

holds that

$$\Lambda(t+T) = \Lambda(t)\boldsymbol{\Xi}, \tag{7.13}$$

whereby $\boldsymbol{\Xi}$ is a constant non-singular matrix.

Let us consider the solution

$$\mathbf{z} = \Lambda(t)\boldsymbol{\xi} = \boldsymbol{\chi}(t) \tag{7.14}$$

of the system (7.10), with $\boldsymbol{\xi}$ as an eigenvector of $\boldsymbol{\Xi}$, i.e.,

$$\det(\boldsymbol{\Xi} - \lambda\mathbf{I}) = \mathbf{0}, \tag{7.15}$$

and λ as its corresponding eigenvalue. Utilizing Eq. (7.13), the solution $\boldsymbol{\chi}(t)$ can be periodically continued as

$$\boldsymbol{\chi}(t+T) = \Lambda(t+T)\boldsymbol{\xi} = \Lambda(t)\boldsymbol{\Xi}\boldsymbol{\xi} = \lambda\boldsymbol{\chi}(t), \tag{7.16}$$

as long as $\lambda = 1$. However, for $\lambda > 1$ the solution is instable since there exist neighbouring paths which are diverging. This behavior is described by the Lyapunov exponent

$$\mu = \frac{1}{T}\lg\lambda, \tag{7.17}$$

i.e., for a positive Lyapunov exponent $\mu > 0$ the system is instable.

http://rcin.org.pl

7.4. Shell segment under periodic forcing

As an example a segment of a cylindrical shell (height $2b = 10\,\mathrm{m}$, segment length $2a = 10\,\mathrm{m}$, thickness $d = 0.1\,\mathrm{m}$, cylinder radius $r = 250/3\,\mathrm{m}$) is investigated. The shell segment is discretized by utilizing triangular shell elements (see Fig. 20). The material properties are given in form of elasticity modulus $Y = 3.4 \cdot 10^{10}\,\mathrm{N/m^2}$, Poisson's ratio $\nu = 0.2$ and mass density $\varrho = 3400\,\mathrm{kg/m^3}$. All edges of the shell segment are restrained in radial direction. The segment is loaded in axial direction by the load p. For a static load of $p_c = 1.65 \cdot 10^6\,\mathrm{N/m}$ the structure has a bifurcation instability. The corresponding buckling shape is depicted in Fig. 21.

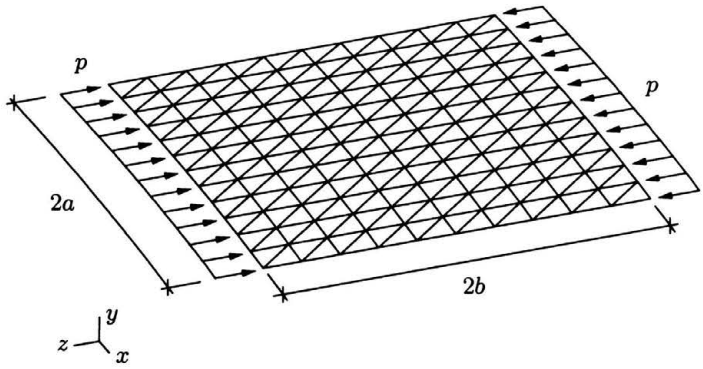

FIGURE 20. Segment of a cylindrical shell under axial loading.

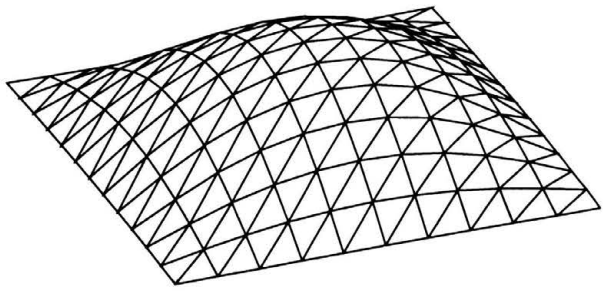

FIGURE 21. Buckling shape under static line load $p_c = 1.65 \cdot 10^6\,\mathrm{N/m}$.

In the following we assume geometrical imperfections in radial direction. In other words, the shell segment shows some deviations from its perfect geometry, however has constant shell thickness. These deviations are modeled as a homogeneous, isotropic, zero-mean, normally ditributed random field

http://rcin.org.pl

with covariance function

$$c(\mathbf{x}_1, \mathbf{x}_2) = \sigma^2 \exp\left[-\frac{\|\mathbf{x}_1 - \mathbf{x}_2\|}{l_c}\right]. \tag{7.18}$$

In Eq. (7.18) $\sigma = 3 \cdot 10^{-3}\,\mathrm{m}$ is the standard deviation of the random field, $l_c = 10\,\mathrm{m}$ is the correlation length and $\mathbf{x}_1$ and $\mathbf{x}_2$ are two coordinates on the cylindrical shell. The support points along the edges are assumed to be deterministic. This is enforced on the random field as a "condition". In Fig. 22 a sample of the unconditional random field is shown, whereas in Fig. 23 a sample conditional on the deterministic support points is shown.

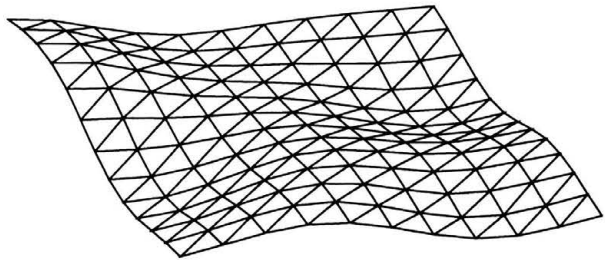

FIGURE 22. Sample of the unconditional random field (display is 400 times magnified).

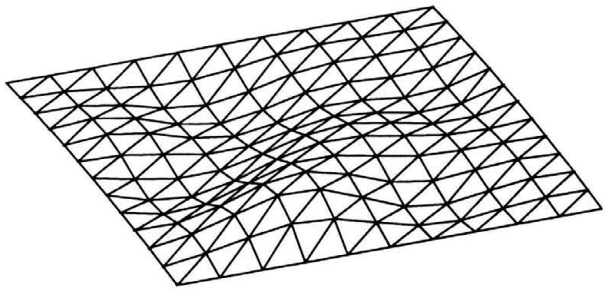

FIGURE 23. Sample of the conditional random field (display is 400 times magnified).

The orthogonal series expansion of the random field results in probabilistically weighted imperfection shapes ϕ_i. The first six imperfection shapes are displayed in Fig. 24. The corresponding variances σ_i^2 are also given. As can be clearly seen, the first imperfection shape shows a high resemblance to the buckling shape. Moreover, its standard deviation is the highest one.

http://rcin.org.pl

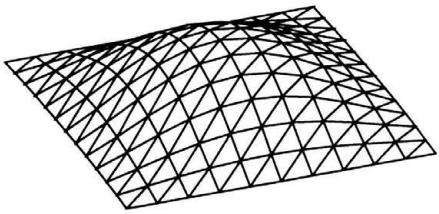

First imperfection shape ($\sigma_1^2 = 6.17$)

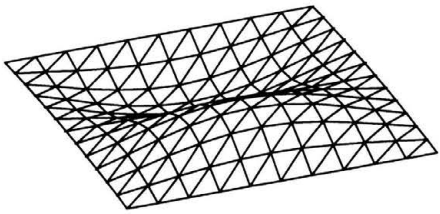

Second imperfection shape ($\sigma_2^2 = 1.82$)

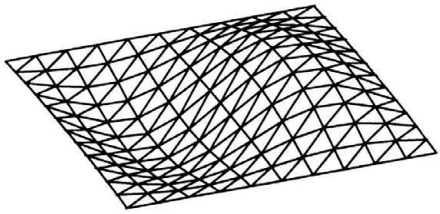

Third imperfection shape ($\sigma_3^2 = 1.82$)

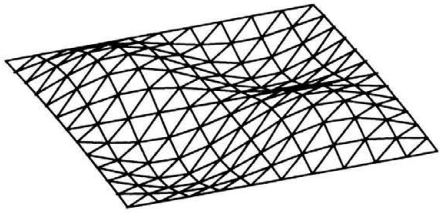

Fourth imperfection shape ($\sigma_4^2 = 0.95$)

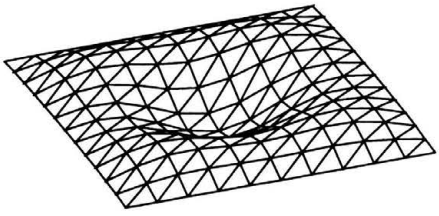

Fifth imperfection shape ($\sigma_5^2 = 0.71$)

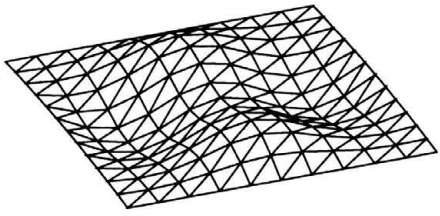

Sixth imperfection shape ($\sigma_6^2 = 0.70$)

FIGURE 24. First six imperfection shapes of the conditional random field (display is 1,500 times magnified).

In the following we assume a periodic load of the form

$$p(t) = 0.77p_c + 0.03p_c \cos(\Omega t), \tag{7.19}$$

whereby the excitation frequency varies in the range $0.5 \leq \Omega/\omega_1 \leq 2.5$, with ω_1 as the first frequency of the undamped, perfect structure under static loading $0.77p_c$. In the following we utilize 12 mode shapes ψ_i for the dynamic analysis. The damping of the structure is assumed to be modeled by

$$\Psi^T \mathbf{C} \Psi = \text{diag}(2i\zeta\omega_i), \qquad i = 1, \ldots, 12, \tag{7.20}$$

http://rcin.org.pl

with $\zeta = 0.02$. The shell segment is stable for all excitation frequencies – as long as there are no geometrical imperfections present.

Taking into account the above given imperfections a slightly different result can be obtained. In Figs. 25 and 26 the Lyapunov exponent is shown as a function of the excitation frequency and the amplitude of the imperfections of the first and third imperfection shape. It can be seen, that for the first imperfaction shape there exists a pronounced dependency between the

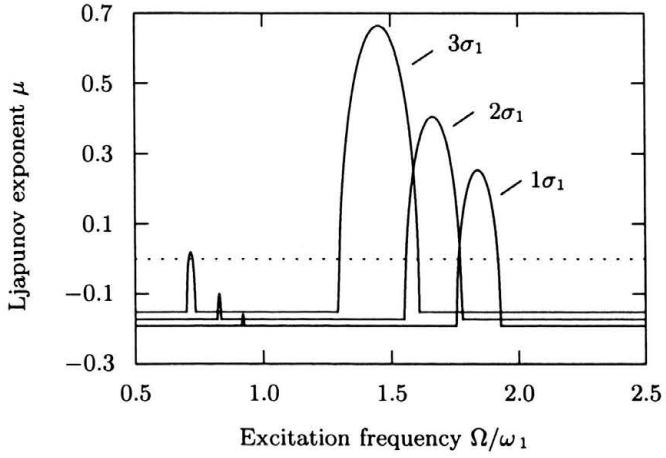

FIGURE 25. Lyapunov exponent as a function of the excitation frequency for the first imperfection shape.

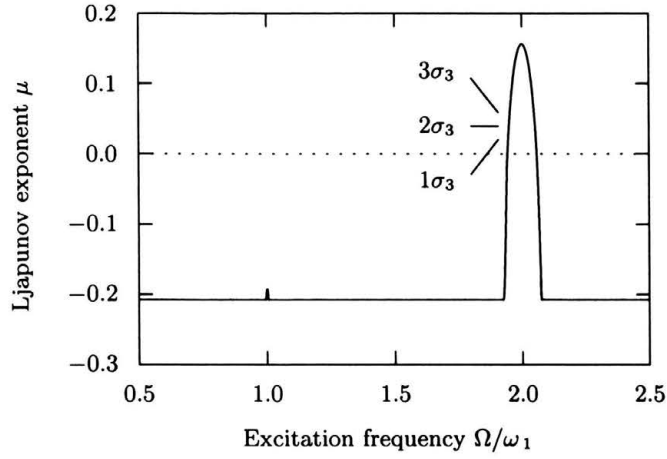

FIGURE 26. Lyapunov exponent as a function of the excitation frequency for the third imperfection shape.

http://rcin.org.pl

Lyapunov exponent and the imperfection amplitude. In other words, with increasing amplitude there are areas of instability ($\mu > 0$) which increase and shift to lower excitation frequencies. In case of the third imperfection shape, however, the Lyapunov exponents are independent of the imperfection amplitude. A similar result as for the third imperfection shape can be achieved for the fifth and sixth imperfection shape. All other imperfection shapes show no visible influence on the Lyapunov exponent. From this follows that for a fully probabilistic analysis only the first, third, fifth and sixth imperfection shape have a significant influence. This allows a considerable reduction in complexity of the calculations as compared to a full modeling of the random field. As methods of calculation variance reduced simulation procedures as described in Sec. 4, or the response surface method, as described in Sec. 5, can be applied.

8. Pre-stressed steel flanges with geometrical imperfections

8.1. Introduction

Recent investigations of pre-stressed flange connections focused on fatigue-relevant tension force amplitudes in the bolts and on failure analysis. These investigations were based on numerous experiments [27, 28, 29, 30, 31]. In [31] a segment of such a flange connection was analyzed by means of finite elements. The results showed a considerable re-distribution of tension forces which leads to a reduction of stress amplitudes in the bolts. An open problem are thereby the geometrical imperfections of the contact surface in the flange. The latter lead to non-uniform distribution of contact pressures and bolt forces, and finally to an increase in tension force amplitudes in the bolts.

Petersen [28] performed an experimental study on these imperfections and derived recommendations for design. Based on a segment model, his conclusions are that the fatigue life is not substantially influenced by imperfections. In contrast, Schmidt et al. [32] based their analysis on quarter- and half-ring flange models. Assuming deterministic imperfection shapes, they show that there is a significant increase in fatigue-relevant stress amplitudes due to deviations from from the perfect geometry. In reality, imperfections are random in location, shape and magnitude. This leads to a loss of structural symmetry. Consequently, a full ring flange model has to be investigated.

8.2. Finite element modeling of flange

A flange connection with an interior ring of 66 bolts (M36) is investigated. The outer diameter of the flange is 3.20 m, the flange thickness is 65 mm

http://rcin.org.pl

and the flange width is 130 mm. The wall thickness of the cylinder shell is 14 mm. The bolts are pre-stressed with a deterministic force of $F_v = 510\,\text{kN}$. For simplicity, only the top flange is modeled, whereas the bottom flange is represented by constraints. The finite element model of the full ring can be seen in Fig. 27. Due to the intended Monte-Carlo-based stochastic analysis the model was chosen in a rather simple way. The model consists of 3,500 elements with 13,000 degrees of freedom. 1,500 non-linear spring elements represent the contact in the flange. These springs have a high stiffness in compression and a low stiffness in tension. Additionally, these elements can have an offset h as shown in Fig. 28. This offset can be utilized to model a gap between the flange surfaces due to imperfect geometry.

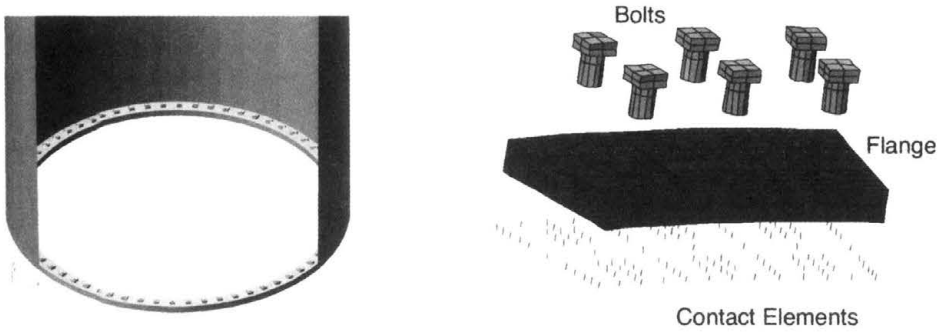

FIGURE 27. Finite element model of the flange.

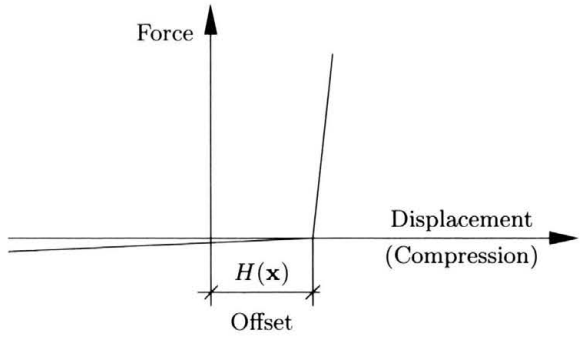

FIGURE 28. Force-displacement relation of contact springs.

In a first step, an analysis with perfect geometry is carried out. The bending moment (as caused, e.g., by wind loading) is increased from 0 MN to 30 MN. The resulting maximum bolt force in the tension zone is shown in Fig. 29. The results compare well to those obtained in [32].

http://rcin.org.pl

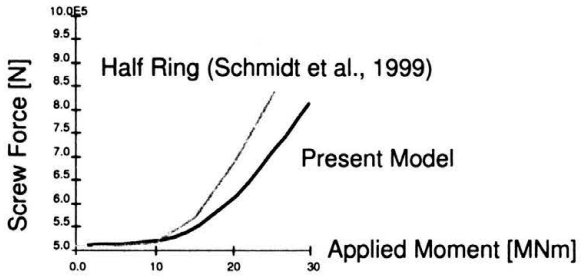

FIGURE 29. Maximum bolt force vs. bending moment.

8.3. Stochastic model of contact surface

A hypothetic stochastic model for the surface assuming a homogeneous and isotropic log-normally distributed random $H(\mathbf{x})$ field is chosen. In the computational procedure, the random field is represented by offsets H_i of the contact springs (see Fig. 28). The random field H has a standard deviation of $\sigma_H = 0.2\,\text{mm}$ and an autocorrelation function

$$c(\mathbf{x}_1, \mathbf{x}_2) = \sigma^2 \exp\left[-\frac{\|\mathbf{x}_1 - \mathbf{x}_2\|}{l_c}\right] \tag{8.1}$$

with a correlation length $l = 200\,\text{mm}$. $\mathbf{x}$ and $\mathbf{y}$ are the Cartesian coordinates in the contact surface. The simulation model is based on a spectral decomposition of the random field [23]. Specific details regarding the treatment of geometrical imperfections are given, e.g., by [33]. Realizations of the random field are obtained by linear combination of the eigenvectors of the covariance matrix with random amplitudes. Three selected eigenvectors (random field mode shapes) are shown in Fig. 30.

Since the model contains 1500 contact elements, the spectral decomposition yields 1500 random field mode shapes. For computational reasons it is useful to reduce this number. A comparative analysis taking into account 800 and 128 random variables was performed. There were virtually no differences in the results. A realization of the contact surface (based on 128 random variables, magnified) is shown in Fig. 31.

For the stochastic analysis it is assumed that the pre-stressing forces in the bolts are deterministic. The initial deformation state for one sample is shown in Fig. 31. Due to the random pressure distribution in the contact zone the application of a bending moment causes random changes in the bolt forces. Based on the Monte Carlo method the statistics of the bolt forces are determined. This requires a nonlinear contact analysis in each simulation. The computational effort can be reduced by applying latin hypercube sampling.

http://rcin.org.pl

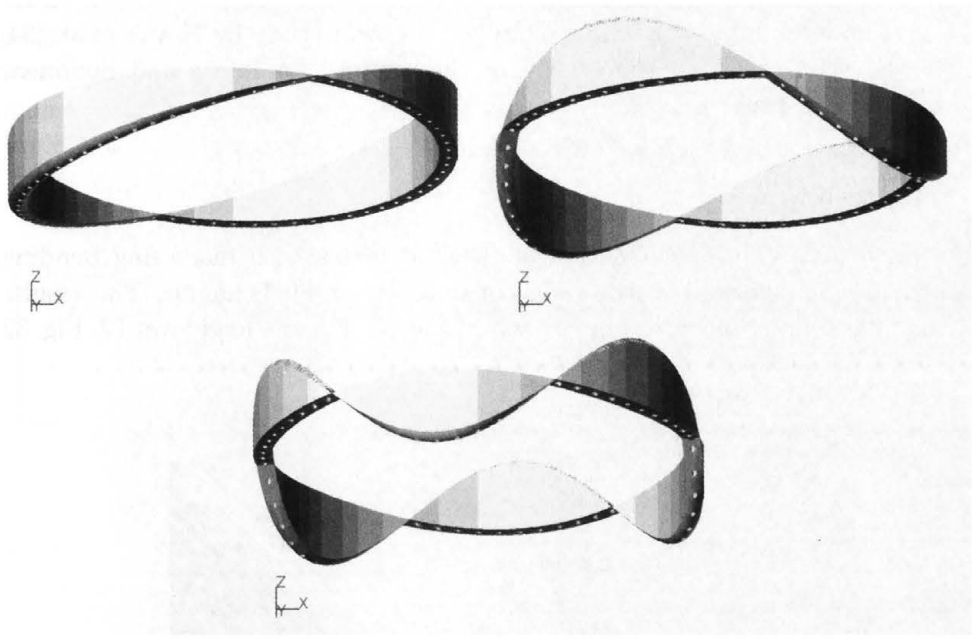

FIGURE 30. Second, fourth and sixth mode shape of random field.

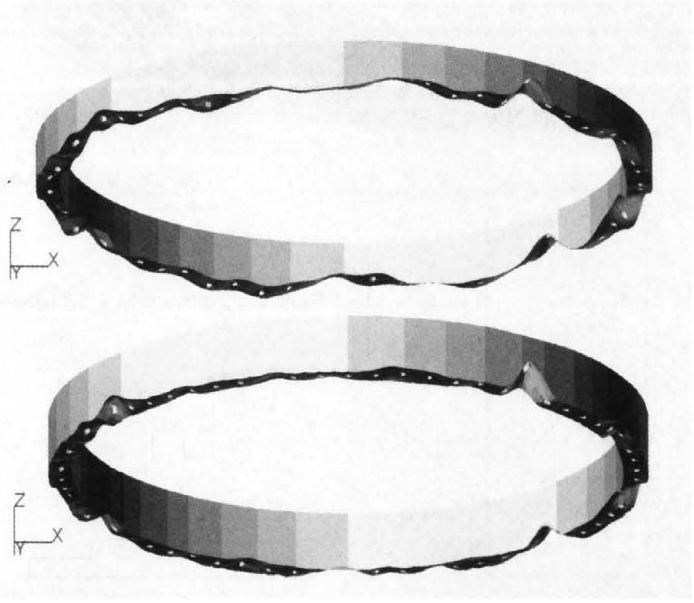

FIGURE 31. Realization of random field (top: initial, bottom: after pre-stressing).

http://rcin.org.pl

This method is particularly useful for estimation of response variability from a very small number of random samples. A recent study by Novák et al. [34] showed the excellent applicability of the method for linear and nonlinear random field problems.

8.4. Results

In a first step, the evolution of the bolt forces with increasing bending moment is monitored in the range of linear material behavior. The results from 300 simulations are summarized in Fig. 32. For the load level 12, Fig. 32

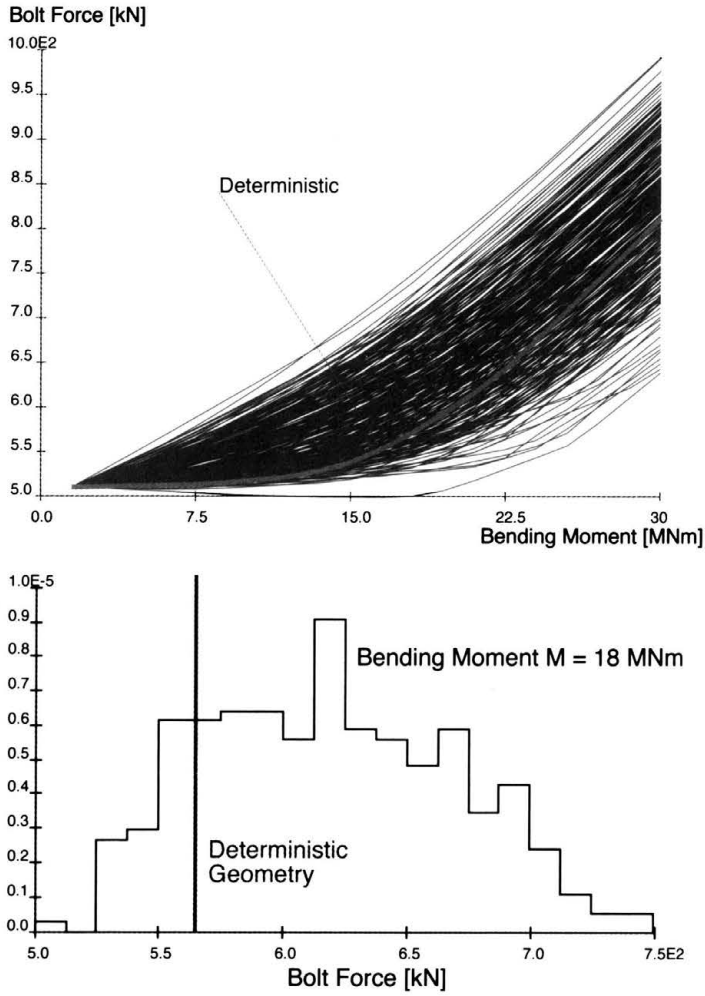

FIGURE 32. Random bolt forces on tension side.

http://rcin.org.pl

shows the histogram of the bolt force on the tension side of the flange ring. Selected results are also summarized in Table 5. The comparison to latin hypercube sampling results from 32 simulations (using 128 random variables) indicate a highly favorable performance of latin hypercube sampling. Figure 33 compares the mean values and standard deviations of the bolt force

TABLE 5. Statistics of bolt forces.

Bending moment [MNm]	Mean force [kN]	C.o.v. [%]	Determ. [kN]
4.5	521	1.5	511
9.0	542	3.7	515
13.5	573	6.1	528
18.0	619	8.1	572

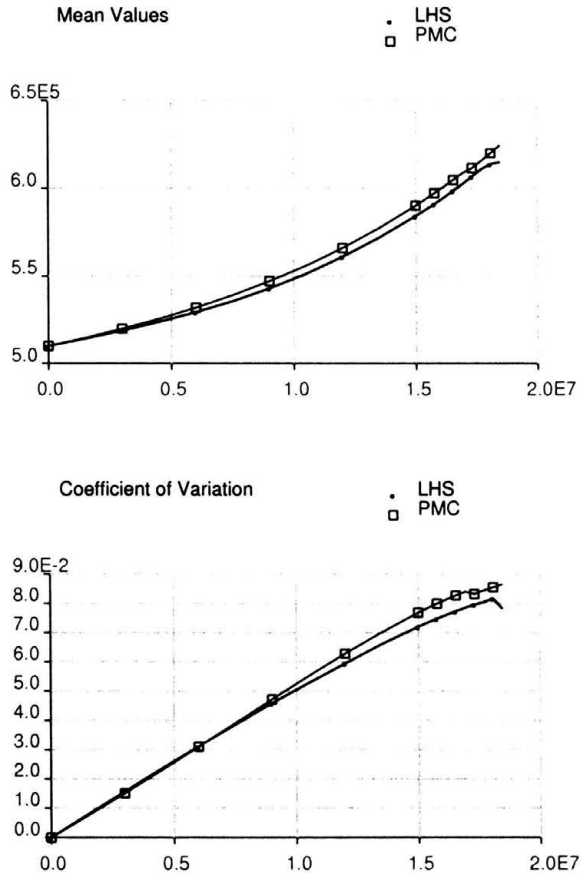

FIGURE 33. Statistics of random bolt forces on tension side vs. bending moment.

http://rcin.org.pl

on the tension side from plain Monte Carlo simulation and latin hypercube sampling. The results are in very good agreement. In a second step, the effect of brittle failure of the bolts on the load carrying capacity of the flange connection was analyzed. Redistribution of the internal forces was taken into account. The ultimate bending moment leading to structural failure showed a significant level of uncertainty with a coefficient of variation of about 8%. Again, the results from latin hypercube sampling with a small sumer of samples are very good as indicated in Table 6.

TABLE 6. Statistics of ultimate bending moment.

Method	Mean Value [MNm]	Coeff. of variation [%]
LHS (32 samples)	22.3	8.7
MCS (200 samples)	21.9	7.6

The results indicate the significance of geometrical imperfections in terms of fatigue life of prestressed flange connections. In addition, also the ultimate bending moment of such a flange is considerably influenced by imperfections. The results are based on a full finite element model of the flange which takes into account the non-uniform initial distributions of stresses in the structure as well as the redistribution due to increased loading. Application of advanced Monte Carlo simulation techniques such as latin hypercube sampling can lead to a substantial reduction of numerical efforts and thus make a stochastic analysis of fairly complex structural systems feasible.

8.5. Experimental investigations

The above mentioned assumptions on the underlying random field are rather hypothetical as yet. They have to be substantiated by means of ex-

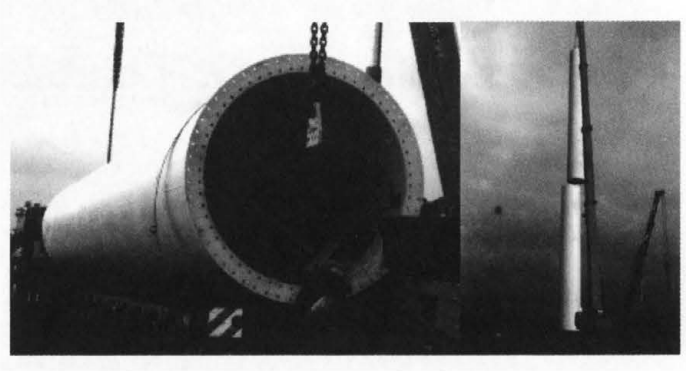

FIGURE 34. Wind turbine tower under construction.

http://rcin.org.pl

perimental investigations. A set of measurements has been carried out and documented by Bucher and Ebert [35]. Photogrammetric measurements were performed on the flange surfaces to determine their exact geometrical shape. The mark-up for the photogrammetry can be seen from Fig. 35. Four representative flange geometries obtained from the measurements are shown in Fig. 36. These smooth geometries were obtained by triangulating the mesh of the measurement points and performing an interpolation using finite plate elements based on static condensation. The geometries can be used as a ba-

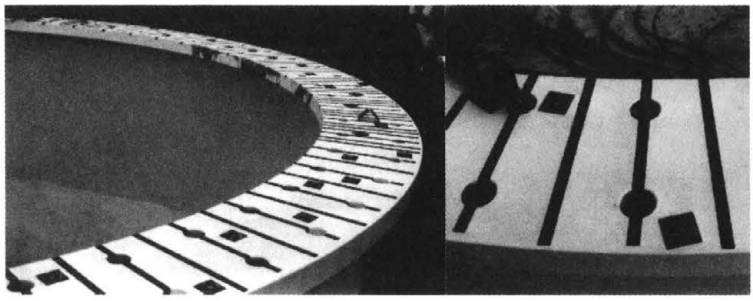

FIGURE 35. Mark-up for photogrammetric measurements.

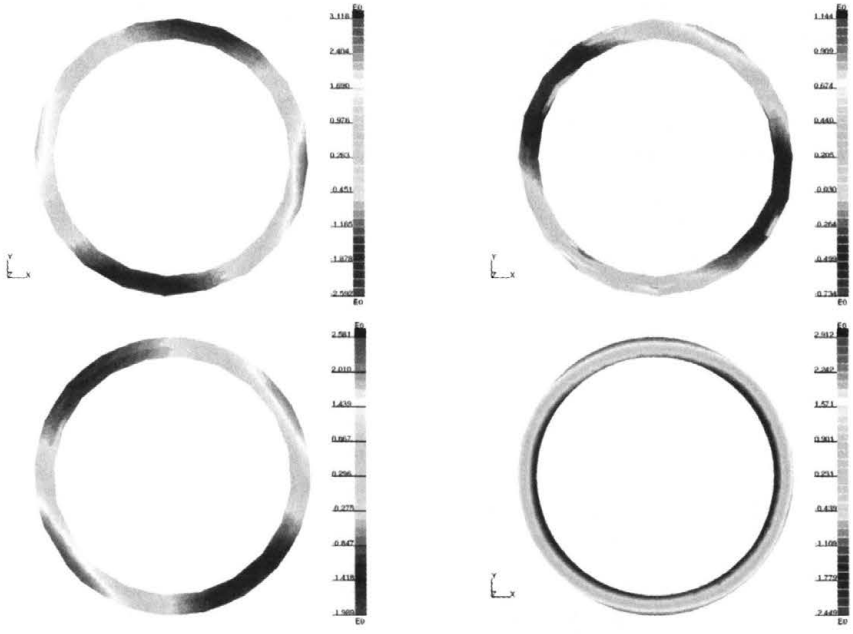

FIGURE 36. Flange geometries (deviations from ideal surface in mm).

http://rcin.org.pl

sis for the further development of random field models for the flange surface. It is quite remarkable that the maximum deviations from the mean surface reach values of 3 mm. This is considerably larger than the standard deviation assumed in the previous calculations. It can therefore be concluded, that even more pronounced effects of the geometrical imperfections may occur in reality.

9. Concluding remarks

The methods available for the analysis of structural reliability allow for a treatment of rather complex random phenomena such as random fields and random processes in conjunction with structural analysis based on the finite element method. It is quite clear that such an analysis – depending on the desired degree of accuracy – requires substantial computing power. This implies that in most realistic situations, due to limitations of computational resources, it may be rather difficult to obtain accurate answers. However, there is a fairly wide choice of approximation methods available to provide reasonably accurate approximations. In particular, approximations based on, e.g., the first order reliability method or the perturbation approach may be quite appropriate for intermediate stages of the reliability analysis such as required during an optimization procedure. Final results may require higher levels of confidence, for which cases importance sampling procedures should be applied.

Acknowledgment

The work reported in this paper has been partially supported by the *Deutsche Forschungsgemeinschaft (DFG)* through *Sonderforschungsbereich 524* which is gratefully acknowledged by the authors.

References

1. A. PAPOULIS, *Probability, Random Variables, and Stochastic Processes*, McGraw-Hill, New York 1991.
2. N. L. JOHNSON, Bivariate distribution based on simple translation systems, *Biometrika*, Vol.36, pp.297–304, 1949.
3. P.-L. LIU and A. DER KIUREGHIAN, Multivariate distribution models with prescribed marginals and covariances, *Probabilistic Engineering Mechanics*, Vol.1, pp.105–112, 1986.
4. C. A. CORNELL, A probability-based structural code, *Journal of the American Concrete Institute*, Vol.66, pp.974–985, 1969.

http://rcin.org.pl

5. P. THOFT-CHRISTENSEN and M. BAKER, *Structural Reliability Theory and Its Applications*, Springer, Berlin 1982.

6. A. M. HASOFER and N. C. LIND, Exact and invariant second-moment code format, *Journal of the Engineering Mechanics Division*, ASCE, Vol.100, pp.111–121, 1974.

7. H. O. MADSEN, S. KRENK and N. C. LIND, *Methods of Structural Safety*, Prentice-Hall, Englewood Cliffs 1986.

8. M. HOHENBICHLER and R. RACKWITZ, Non-normal dependent vectors in structural safety, *Journal of the Engineering Mechanics Division*, ASCE, Vol.107, pp.1227–1238, 1981.

9. M. SHINOZUKA, Basic analysis of structural safety, *Journal of Structural Engineering*, ASCE, Vol.109, pp.721–740, 1983.

10. J. M. HAMMERSLEY and D. C. HANDSCOMB, *Monte Carlo Methods*, Methuen, London 1964.

11. R. Y. RUBINSTEIN, *Simulation and the Monte Carlo Method*, Wiley, New York 1981.

12. C. G. BUCHER, Adaptive sampling – An iterative fast Monte Carlo procedure, *Structural Safety*, Vol.5, pp.119–126, 1988.

13. R. RACKWITZ, *Response Surfaces in Structural Reliability*, Berichte zur Zuverlässigkeitstheorie der Bauwerke, Heft 67, TU München, München 1982.

14. G. E. P. BOX and N. R. DRAPER, *Empirical Model-Building and Response Surfaces*, Wiley, New York 1987.

15. R. H. MYERS and D. C. MONTGOMERY, *Response Surface Methodology: Process and Product Optimization Using Designed Experiments*, Wiley, New York 2002.

16. F. BÖHM and A. BRÜCKNER-FOIT, On criteria for accepting a response surface model, *Probabilistic Engineering Mechanics*, Vol.7, pp.183–190, 1992.

17. A. I. KHURI and J. A. CORNELL, *Response Surfaces: Designs and Analyses*, Dekker, New York 1996.

18. C. G. BUCHER and U. BOURGUND, A fast and efficient response surface approach for structural reliability problems, *Structural Safety*, Vol.7, pp.57–66, 1990.

19. S.-H. KIM and S.-W. NA, Response surface method using vector projected sampling points, *Structural Safety*, Vol.19, pp.3–19, 1997.

20. Y. ZHENG and P. K. DAS, Improved response surface method and its application to stiffened plate reliability analysis, *Engineering Structures*, Vol.22, pp.544–551, 2000.

21. H. G. MATTHIES, C. E. BRENNER, C. G. BUCHER and C. G. SOARES, Uncertainties in probabilistic numerical analysis of structures and solids – Stochastic finite elements, *Structural Safety*, Vol.19, pp.283–336, 1997.

22. H. G. MATTHIES and C. BUCHER, Finite elements for stochastic media problems, *Computer Methods in Applied Mechanics and Engineering*, Vol.168, pp.3–17, 1999.

23. R. G. GHANEM and P. D. SPANOS, *Stochastic Finite Elements: A Spectral Approach*, Springer, Berlin 1991.

24. C. E. BRENNER, *Ein Beitrag zur Zuverlässigkeitsanalyse von Strukturen unter Berücksichtigung von Systemunsicherheiten mit Hilfe der Methode der Stochastischen Finiten Elemente*, Dissertation, Universität Innsbruck, Innsbruck, 1995.

http://rcin.org.pl

25. *SLang - The Structural Language Version 5.0, User's Manual*, Institut für Strukturmechanik, Bauhaus-Universität Weimar, Weimar 2003.

26. O. DITLEVSEN, Random field interpolation between point by point measured properties, in: *Proc. 1st Int. Conf. on Computational Stochastic Mechanics, Corfu, Greece, September 17–19, 1991*, (P. D. Spanos and C. A. Brebbia, Eds.), pp.801–812, Computational Mechanics Publications, Southampton 1991.

27. C. PETERSEN, *Stahlbau*, Vieweg, Braunschweig 1990.

28. C. PETERSEN, Tragfähigkeit imperfektionsbehafteter geschraubter Ringflanschverbindungen, *Stahlbau*, Vol.59, pp.97–104, 1990.

29. H. SCHMIDT and M. NEUPER, Zum elastostatischen Tragverhalten exzentrisch gezogener L-Stöße mit vorgespannten Schrauben, *Stahlbau*, Vol.66, pp.163–168, 1997.

30. C. PETERSEN, Nachweis der Betriebsfestigkeit exzentrisch beanspruchter Ringflanschverbindungen, *Stahlbau*, Vol.67, pp.191–203, 1998.

31. M. EBERT and C. BUCHER, Stochastische nichtlineare Untersuchung vorgespannter Schraubenverbindungen unter Windeinwirkung, in: *Baukonstruktionen unter Windeinwirkung*, (U. Peil, Ed.), pp.175–184, WTG-Bericht Nr. 5, Aachen 1998.

32. H. SCHMIDT and T. WINTERSTETTER and M. KRAMER, Nonlinear elastic behaviour of imperfect, eccentrically tensioned L-flange ring joints with prestressed bolts as basis for the fatigue design, in: *Proc. European Conference on Computational Mechanics*, CD-ROM, Munich 1999.

33. Y. SCHORLING and C. BUCHER, Stochastic stability of structures with random imperfections, in: *Stochastic Structural Dynamics*, (B. F. Spencer, Jr. and E. A. Johnson, Eds.), pp.343–348, Balkema, Rotterdam 1999.

34. D. NOVÁK, W. LAWANWISUT and C. BUCHER, Simulation of random fields based on orthogonal transformations of covariance matrix and latin hypercube sampling for SFEM, in: *Proc. Int. Conf. on Monte Carlo Simulation, Monte Carlo, Monaco, June 18–21, 2000*, (G. I. Schuëller and P. D. Spanos, Eds.), Balkema, Rotterdam 2001.

35. C. BUCHER and M. EBERT, Nichtlineare Berechnung von Stahlflanschverbindungen mit gemessenen Imperfektionen, *Stahlbau*, Vol.71, pp.516-522, 2002.

http://rcin.org.pl